

An A_4 -Symmetric Double Seesaw for Neutrino Masses and Mixing in Light of JUNO results

Swaraj Kumar Nanda^{a*}, Maibam Ricky Devi^{b†}, Chandini Dash^{c‡}
 R.N. Panda^{a§}, Sudhanwa Patra^{d,e¶}

^a Department of Physics, ITER, SOA University, Bhubaneswar-751030, India

^b Department of Physics, Gauhati University, Guwahati-781014, India

^c Department of Physics, Utkal University, Vani Vihar, Bhubaneswar-751004, India

^d Department of Physics, Indian Institute of Technology Bhilai, Durg-491002, India

^e Institute of Physics, Sachivalaya Marg, Bhubaneswar-751005, India

Abstract

We discuss a double seesaw mechanism for generating light neutrino masses within the Standard Model extensions that include both right-handed neutrinos and extra gauge-singlet sterile fermions. The flavour structure of the double seesaw framework is invoked by an A_4 discrete symmetry which yields predictive textures for the Dirac neutrino mass matrix M_D , the mixing matrix M_{RS} connecting right-handed and sterile neutrinos, and the bare Majorana mass matrix M_S for the sterile neutrinos. After different A_4 charge assignments for the left-handed lepton doublets, the right-handed neutrinos, and the sterile neutrinos, we consider simple flavon vacuum alignments that can provide highly constrained and phenomenologically interesting mass structures relevant for generating light neutrino masses via the double seesaw mechanism. The interesting feature of the present framework is that the combination of the double seesaw mechanism and A_4 flavour alignments yields a leading-order tribimaximal (TBM) structure, corrected by a single rotation in the (1-3) sector. The resulting correction is responsible for generating the experimentally observed value of θ_{13} while retaining the approximate TBM predictions for θ_{12} and θ_{23} . We then derive analytic expressions for the heavy sterile eigenvalues and for the resulting light neutrino masses, thereby clarifying the role of the symmetry in shaping the neutrino mass hierarchy. We further incorporate the most recent JUNO measurements, which improve the precision of the solar mixing angle $\sin^2 \theta_{12} \simeq 0.31$, along with updated constraints on $\sin^2 \theta_{13}$. We show that these results significantly restrict the allowed parameter space of the model. In particular, the observed value of $\sin^2 \theta_{12}$ constrains the magnitude of the (1-3) rotation and the phases associated with the A_4 flavon couplings, while the value of $\sin^2 \theta_{13}$ sharpens these restrictions further. Overall, the interplay between double seesaw dynamics, A_4 flavour symmetry, and the recent JUNO constraints yields a highly predictive framework for neutrino masses and mixings, offering a coherent explanation for the generation of light neutrino masses and providing testable predictions for future experiments.

*swarajnanda.phy@gmail.com

†deviricky@gmail.com

‡dash25chandini@gmail.com

§rabinarayanpanda@soa.ac.in

¶sudhanwa@iitbhilai.ac.in

Contents

1	Introduction	2
2	Theoretical Framework	4
2.1	Double Seesaw Mechanism	4
2.1.1	Diagonalization scheme for DSM	5
2.2	A_4 implementation of Double Seesaw Mechanism	6
2.2.1	Flavon alignments and structure of mass matrices	7
3	Predictive structure of mass matrices for double seesaw framework	8
3.1	Diagonal and degenerate structure of M_D and M_{RS}	10
3.1.1	Mass spectra and normalization	13
4	Mixing Structure from A_4: Tribimaximal Form and a Single Complex Rotation	14
4.1	Diagonalization of the 1–3 Block and Physical Parameterization	16
4.2	Special Limits and Physical Interpretation	17
4.3	Derivation of Double Seesaw Neutrino Masses in the Degenerate Yukawa Limit	18
5	Numerical Analysis and Constraints on Model Parameters	19
5.1	For Normal Ordering	19
5.2	For Inverted Ordering	22
6	Results and Discussion: A_4-Symmetric Double Seesaw	24
6.1	Impact on Solar Neutrino Parameters from JUNO first data and other experimental solar measurements	28
6.2	Impact on Atmospheric Neutrino Parameters from atmospheric data from Deep Core Ice-Cube and LBL experiments	31
6.3	Synergy between mixing angles and phases	31
6.4	Neutrinoless Double Beta Decay Implications from JUNO data	34
6.5	Correlation between Dirac CP Phase and Jarlskog Invariant	36
7	Conclusion	37
A	Predictive Structures of the Double Seesaw Mechanism with A_4 Symmetry	39
B	Detailed Derivation of Mass and Mixing Structure in the Double Seesaw Framework with A_4 Symmetry	41
C	Flavon Potential and Vacuum Alignment	43
D	Detailed Derivation of Mixing Angles and CP Phases	45

1 Introduction

The Standard Model (SM) of particle physics has been remarkably successful in describing the electromagnetic, weak, and strong interactions among the elementary particles and almost all of its predictions have been verified to high precision scale in numerous experiments, culminating in the latest discovery of the Higgs boson at the Large Hadron Collider (LHC). Despite the remarkable success of the Standard Model (SM) in describing particle physics up to the electroweak scale, it fails to address many fundamental questions at very theoretical as well as experimental level. The theoretical origin of neutrino masses and mixing remains an outstanding question among one of them. The discovery of neutrino oscillations has firmly established that neutrinos are massive and mix with one another, which is confirmed from various experiments [1–4]. These results constitute the first experimental evidence of physics beyond the Standard Model while SM cannot accommodate massive neutrinos in its minimal form.

The most popular canonical (or Type-I) seesaw mechanism provides a natural way to explain the tiny neutrino masses through the introduction of right-handed neutrinos singlets under SM gauge symmetry [5–8]. The Type-I seesaw is perhaps the simplest and most well-studied framework for generating Majorana neutrino masses. It extends the Standard Model by adding heavy right-handed neutrino fields N_{Ri} ($i = 1, 2, 3$), which are singlets under the SM gauge group $SU(2)_L \times U(1)_Y$. These fields allow the construction of both Dirac and Majorana mass terms. The Type-I seesaw mechanism thus provides a minimal and elegant explanation of neutrino mass generation, embedding naturally in grand unified theories (GUTs) such as $SO(10)$, where right-handed neutrinos appear automatically in the 16 representation. Moreover, the heavy Majorana neutrinos introduced in this framework can decay out of equilibrium in the early Universe, generating a lepton asymmetry that is later converted into the observed baryon asymmetry through sphaleron processes, providing a natural realization of leptogenesis [9]. Alternatively, the type-II [10–14] and type-III [15, 16] offers an alternative explanation for the origin of neutrino masses by introducing a scalar triplet field Δ transforming as $(1, 3, 1)$ (fermion triplet $\Sigma(1, 3, 0)$) under the SM gauge group. Along with the origin and smallness of neutrino masses, the observed pattern of lepton mixing, mass hierarchy [17–19] and its nature - whether Dirac [20] or Majorana type [21], remain among the most significant questions in neutrino physics.

The limitation with the canonical seesaw mechanism is that the sub-eV scale of light neutrino masses is linked to a very high scale right-handed neutrinos which is beyond the reach of current or planned experiments. Alternatively, the seesaw scale can be lowered down to TeV range viable for LHC or lowe energy phenomenology within inverse seesaw or linear seesaw variants [22–32]. In this context, the double seesaw mechanism [33, 34] comes with added advantage while resulting an additional layer of suppression through extra singlet fermions, allowing for a lower seesaw scale. In comparison to the usual inverse or linear seesaw mechanism where the light neutrinos are Majorana and heavy neutrinos form pseudo-Dirac pair whereas the double seesaw is attractive in the sense that it naturally accommodates very small Majorana neutrino masses for light neutrinos while allowing large Majorana masses for the heavy states to be at intermediate scales or at TeV scale offering the exciting possibility

of testing neutrino mass generation and leptogenesis mechanisms at current or near-future experiments phenomenology [35–39].

Recently, JUNO measurement for neutrino oscillation parameters has hinted possible implications for the lepton mixing patterns and its possible origin from non-Abelian discrete flavour symmetries with the predictions for $\sin^2 \theta_{12}$ [40, 41]. In the other hand, the role of discrete flavor symmetries in neutrino model building has been studied over the last two decades with the most popular A_4 group due to its minimal irreducible triplet representation that can naturally accommodate three fermion generations. Thus, the interesting results from JUNO motivated us to revisit A_4 based flavor models in the context of seesaw variants, in particular, the double seesaw for simultaneous explanation of light neutrino masses, neutrinoless double beta decay and its potential to address matter-antimatter asymmetry of the universe via decay of right-handed neutrinos. Original works of A_4 models have been shown to naturally yield the tribimaximal (TBM) mixing pattern while subsequent works introduced all suitable corrections to accommodate the measured non-zero reactor mixing angle. Incorporating seesaw mechanisms within A_4 frameworks has been central idea to explain small light neutrino masses and mixing patterns while ensuring predictivity in the Yukawa sector. The type-I realizations with A_4 flavon alignments [42–44] have been shown to generate viable neutrino mixing consistent with oscillation data providing correlations among angles and CP-phase along with testable predictions for neutrinoless double beta decay. Recent extensions to modular symmetries, particularly, modular A_4 , have gained attention in neutrino community as they can reduce the need of multiple flavons and yeild highly constrained parameters spaces [45–55]

Despite all these progresses made, relatively little attention has been paid to the double seesaw mechanism within A_4 framework. In the present work, we explore the implementation of the double seesaw mechanism within an A_4 flavor symmetric extension of the Standard Model. By assigning appropriate A_4 representations to the left-handed lepton doublets, right-handed neutrinos, and sterile fermions, and by introducing modular forms or flavon fields transforming under A_4 , we construct the neutrino mass matrices M_D , M_{RS} , and M_S through the invariant Yukawa Lagrangian. The double seesaw offers a natural explanation of the smallness of light neutrino masses by introducing double layer of suppression through a hierarchy $M_S \gg M_{RS} \gg M_D$ leading to the new mass formula for right-handed neutrinos $M_R \simeq -M_{RS}M_S^{-1}M_{RS}^T$ and double seesaw formula for light neutrinos as $m_\nu \simeq -M_D M_R^{-1} M_D^T$. This framework not only accommodates a wide range of Majorana masses for heavy-neutrinos, starting from eV scale to GUT scale, but also enables natural conditions for quasi-degenerate right-handed neutrinos at the few GeV scale, which are particularly attractive for low-scale resonant leptogenesis. Unlike in minimal type-I seesaw mechanism that usually requires ultra-heavy scale or fine-tuned parameter space, the A_4 implemented double seesaw has multi-fold phenomenology: (i) provides a natural origin of light neutrino masses via the double seesaw suppression without invoking extremely heavy right-handed neutrinos or additional fine-tuning, (ii) A_4 flavor symmetry constrains the form of the mass matrices, leading to predictive structures consistent with current oscillation data, (iii) the framework allows for low-scale or resonant leptogenesis, thereby linking the generation of the baryon asymmetry of the Universe with the flavor structure of the neutrino

sector. Within appropriate choice of parameter space, the double seesaw framework can remain within reach of laboratory and cosmological tests.

This paper is organized as follows. In Sect. 2 we define the theoretical framework including field content and mass matrices of the double seesaw framework, while presenting explicit flavon-driven constructions that yield the structure of masses matrices relevant for neutrino masses and mixing analysis. Sec. 3 contains analytic diagonalization of mass matrices and useful closed forms for eigenvalues. In Sec. 4 we discuss the tribimaximal form and single complex rotation. Sec. 5 defines confrontation with oscillation data, neutrinoless double beta decay and prospects for leptogenesis. Sec. 6 outlines result and discussion. We conclude in Sec. 7. Appendices collect formulae and alternative assignment tables.

2 Theoretical Framework

2.1 Double Seesaw Mechanism

The double seesaw mechanism is an elegant extension of the canonical Type-I seesaw that naturally explains the smallness of light neutrino masses through the inclusion of additional gauge-singlet fermions. In this framework, the Standard Model (SM) neutrinos ν_L couple to the right-handed neutrinos N_R through the Dirac mass matrix M_D , while N_R further couple to additional sterile fermions S_L via another mass term M_{RS} . The sterile states S_L acquire their own small Majorana mass term M_S , which explicitly breaks lepton number at a very high scale.

To implement the double seesaw framework for generating a sub-eV scale of light neutrino masses, we extend the minimal lepton sector of the Standard Model with three generations of heavy right-handed neutrinos N_R and left-handed sterile neutrinos S_L . In the flavor basis (ν_L, N_R^c, S_L) , the general form of double seesaw mass matrix structure is as follows,

$$\mathbb{M}_{\text{DSM}} = \begin{pmatrix} 0 & M_D & 0 \\ M_D^T & 0 & M_{RS} \\ 0 & M_{RS}^T & M_S \end{pmatrix}. \quad (2.1)$$

where, M_D is the 3×3 Dirac neutrino mass matrix (connecting ν_L and N_R), M_{RS} is the mixing mass matrix connecting N_R and S_L , and M_S is the bare Majorana mass matrix for the singlets S_L . We assume the hierarchy

$$M_S \gg M_{RS} \gg M_D, \quad (2.2)$$

which is relevant for double seesaw mechanism. Assuming the hierarchy $M_S \gg M_{RS} \gg M_D$, the light neutrino masses arise through a two-step seesaw approximations: (i) first integrating out heavy sterile neutrinos, (ii) subsequently, integrating out the intermediate heavy right-handed neutrinos. Using this double seesaw method one can obtain the mass matrices for the light, intermediate heavy right-handed and heaviest sterile neutrinos as,

$$m_\nu = M_D (M_{RS}^{-1})^T M_S M_{RS}^{-1} M_D^T, \quad (2.3)$$

$$m_N = M_R, \quad (2.4)$$

$$m_S = M_S. \quad (2.5)$$

2.1.1 Diagonalization scheme for DSM

In the double seesaw mechanism, the diagonalization of the neutral fermion mass matrix can be carried out by applying successive block diagonalization procedure. Here the block diagonalization of the mass matrix includes two-step seesaw approximation.

Step-1: First Seesaw Approximation:-

In the first step of seesaw approximations, we are integrating out the heaviest singlets S_L and express the effective 6×6 mass matrix for (ν_L, N_R^c) neutral fermions. We follow the seesaw approximations adopted in Ref. [56] and the DSM mass matrix for double seesaw mechanism can be written in the standard form of Type-I+II seesaw as,

$$\mathbb{M}_{\text{DSM}} = \begin{pmatrix} 0 & M_D & 0 \\ M_D^T & 0 & M_{RS} \\ 0 & M_{RS}^T & M_S \end{pmatrix} \equiv \begin{pmatrix} \mathbb{M}_L & \mathbb{M}_D \\ \mathbb{M}_D^T & \mathbb{M}_R \end{pmatrix},$$

where, $\mathbb{M}_L = \begin{pmatrix} 0 & M_D \\ M_D^T & 0 \end{pmatrix}$, $\mathbb{M}_D = \begin{pmatrix} 0 \\ M_{RS} \end{pmatrix}$, $\mathbb{M}_R = M_S$. (2.6)

With the modified mass hierarchy $|\mathbb{M}_R| \gg |\mathbb{M}_D| \gg |\mathbb{M}_L|$ and using the standard results of type-I+II seesaw approximation, the effective block diagonalized mass matrix in the basis of (ν_L, N_R^c) is given by

$$\begin{aligned} \mathbb{M}_{\nu N} &= \mathbb{M}_L - \mathbb{M}_D \mathbb{M}_R^{-1} \mathbb{M}_D^T \\ &= \begin{pmatrix} 0 & M_D \\ M_D^T & 0 \end{pmatrix} - \begin{pmatrix} 0 \\ M_{RS} \end{pmatrix} M_S^{-1} \begin{pmatrix} 0 & M_{RS}^T \end{pmatrix} \\ &= \begin{pmatrix} 0 & M_D \\ M_D^T & -M_{RS} M_S^{-1} M_{RS}^T \end{pmatrix}, \end{aligned} \quad (2.7)$$

and the resulting mass formula for integrated heaviest sterile neutrinos is given by

$$m_S = M_S. \quad (2.8)$$

Step-2: Second Seesaw Approximation:-

After integrating out the heavy sterile neutrinos by following the first seesaw approximation, the resulting effective mass matrix given in Eq.(2.9) is exactly in the form of usual type-I seesaw form as,

$$\mathbb{M}_{\nu N} = \begin{pmatrix} 0 & M_D \\ M_D^T & -M_{RS} M_S^{-1} M_{RS}^T \end{pmatrix} \equiv \begin{pmatrix} 0 & \mathcal{M}_D \\ \mathcal{M}_D^T & \mathcal{M}_R \end{pmatrix} \quad (2.9)$$

with $\mathcal{M}_D = M_D$ and $\mathcal{M}_R = -M_{RS} M_S^{-1} M_{RS}^T$. Using the allowed mass hierarchy given in Eq.(2.2), we can get $|-M_{RS} M_S^{-1} M_{RS}^T| \gg |M_D|$ which can be applicable for this modified type-I seesaw form displayed in Eq.(2.9). Thus, one can apply seesaw approximations once

more, the right-handed neutrinos are integrated out and the resulting mass formula for the light left-handed neutrinos is given below:

$$\begin{aligned} m_\nu &= -\mathcal{M}_D \mathcal{M}_R^{-1} \mathcal{M}_D^T = -M_D \left(-M_{RS} M_S^{-1} M_{RS}^T \right)^{-1} M_D^T \\ &= M_D (M_{RS}^{-1})^T M_S M_{RS}^{-1} M_D^T. \end{aligned} \quad (2.10)$$

Similarly, the resulting mass formula for integrated intermediate heavy right-handed neutrinos is given by

$$m_N = M_R = -M_{RS} M_S^{-1} M_{RS}^T. \quad (2.11)$$

2.2 A_4 implementation of Double Seesaw Mechanism

We briefly discuss the A_4 implementation of double seesaw mechanism with minimal extension of SM with three generations of right-handed neutrinos N_{R_i} , three sterile neutrinos S_{L_i} , scalar flavons $\phi_T, \phi_S, \xi, \xi'$ that break A_4 symmetry, and the SM Higgs doublet. We also summarize the field transformations of various fields under the SM gauge group $SU(2)_L \times U(1)_Y$ and A_4 flavor symmetry used in our DSM construction presented in Table 1. The role of A_4 flavor symmetry is two fold: (i) it forbids arbitrary mass matrix structures and thereby constraining the Dirac and Majorana mass terms; (ii) it provides a correlated mass matrices such that the resulting double seesaw generated light neutrino mass matrix is essentially governed by the sterile neutrino mass matrix and a scale factor.

Field	$SU(2)_L$	$U(1)_Y$	A_4	Comment
ℓ_L	2	-1/2	1, 1', 1''	Left-handed leptons
e_R	1	-1	1, 1', 1''	Charged leptons
N_R	1	0	1, 1', 1''	Right-handed neutrinos
S_L	1	0	3	Sterile neutrinos
H	2	1/2	1	SM Higgs
$\phi_T, \phi_S, \xi, \xi'$	1	0	Flavons (3, 3, 1, 1')	Break A_4

Table 1: Representative field assignments under A_4 (and SM gauge group).

We choose a minimal A_4 transformation in all fields relevant for the implementation of the double seesaw mechanism by assigning single one dimensional A_4 representations to the left-handed lepton doublets, right-handed charged leptons e_R , and right-handed neutrinos N_R transforming as 1, 1', 1'' as presented in Table 1. The sterile neutrinos S_L transform under this A_4 group as a triplet 3. Here, A_4 invariant Lagrangian for implementation of the double seesaw mechanism is given by

$$\begin{aligned} \mathcal{L}_{\text{DSM}} &= \mathcal{L}_{M_D} + \mathcal{L}_{M_{RS}} + \mathcal{L}_{M_S} \\ \text{where, } \mathcal{L}_{M_D} &= \alpha_D \overline{\ell_{eL}} \tilde{H} N_{R1} + \beta_D \overline{\ell_{\mu L}} \tilde{H} N_{R2} + \gamma_D \overline{\ell_{\tau L}} \tilde{H} N_{R3} + h.c. \\ \mathcal{L}_{M_{RS}} &= \alpha_{RS} \overline{N_{R1}} (S_L \phi_T)_1 + \beta_{RS} \overline{N_{R2}} (S_L \phi_T)_{1'} + \gamma_{RS} \overline{N_{R3}} (S_L \phi_T)_{1''} + h.c. \\ \mathcal{L}_{M_S} &= (\alpha_S \phi_S + \beta_S \xi + \gamma_S \xi') \overline{S_L^c} S_L + h.c. \end{aligned} \quad (2.12)$$

Additionally, we present, here, Lagrangian term for charged lepton mass matrix as,

$$\mathcal{L}_{M_\ell} = \alpha_\ell \overline{\ell_{eL}} H e_R + \beta_\ell \overline{\ell_{\mu L}} H \mu_R + \gamma_\ell \overline{\ell_{\tau L}} H \tau_R + h.c. \quad (2.13)$$

2.2.1 Flavon alignments and structure of mass matrices

The vacuum alignment of different flavon fields breaking A_4 symmetry is very important for flavor structure of various mass matrices involved in double seesaw mechanism (see Appendix C) [57–60]. The tree level bare Majorana mass term for light neutrinos and right-handed neutrinos are either not allowed or forbidden by some symmetry. The Majorana mass term for left-handed light neutrinos are not allowed by SM gauge symmetry while the Majorana mass term for right-handed neutrinos and mixing term between light active and heavy sterile neutrinos are forbidden by imposing a global $U(1)_X$ symmetry or with discrete symmetry, say $Z_4 \times Z_2$.

VEV alignments for diagonal M_D and M_{RS} :

$$\langle \phi_T \rangle = v_T(1, 0, 0), \quad \langle \phi_S \rangle = v_S(1, 1, 1), \quad \langle \xi \rangle = u, \quad \langle \xi' \rangle = u'$$

With suitable flavon vacuum expectation values (VEVs) as discussed in the Appendix C, the following minimal and predictive textures of mass matrices are constructed as follows:

- **Dirac neutrino mass matrix M_D :** Using A_4 assignment of left-handed lepton doublets $\{l_{eL}, l_{\mu L}, l_{\tau L}\}$ and right-handed neutrinos $\{N_{R1}, N_{R2}, N_{R3}\}$ as $1, 1', 1''$ as presented in Table.1, the derived structure of Dirac neutrino mass matrix M_D is diagonal as

$$M_D = v \text{ diag}(\alpha_D, \beta_D, \gamma_D) \quad (2.14)$$

where, $\langle H \rangle = v$ is the electroweak VEV. With the above assignments, the Dirac mass matrix is diagonal at leading order and may even reduce to an identity matrix if $\alpha_D = \beta_D = \gamma_D \equiv k_D$. This results from the trivial contraction of A_4 singlets without the need for additional flavons.

- **Right-sterile mixing mass matrix M_{RS} :** The mixing term between the right-handed neutrinos and the sterile neutrinos (M_{RS}) is forbidden at tree level by appropriate choice of A_4 assignment. The coupling of right-handed neutrinos to sterile fermions proceeds only through flavon insertions. After vacuum alignment, M_{RS} is also diagonal, and in our present analysis, proportional to M_D . This alignment is central to the “screening mechanism” to be used for double seesaw mechanism which will be discussed in the later section of neutrino masses and mixing. The diagonal structure of M_{RS} after suitable VEV alignment as,

$$M_{RS} = v_T \text{ diag}(\alpha_{RS}, \beta_{RS}, \gamma_{RS}), \quad (2.15)$$

Similarly, the mass matrix M_{RS} is considered to be diagonal at leading order and may even reduce to an identity matrix if $\alpha_{RS} = \beta_{RS} = \gamma_{RS} \equiv k_{RS}$.

- **Sterile Majorana mass matrix M_S :** The sterile neutrinos $\{S_{L1}, S_{L2}, S_{L3}\}$ are transforming as A_4 triplet and the sterile Majorana mass matrix is flavon-dominated and admits the typical structure diagonalized by U_{TBM} with small U_{13} corrections. This is mainly because of the ratio M_D/M_{RS} is proportional to an identity matrix under screening condition of M_D and M_{RS} assumed in our analysis thereby, the double seesaw mass formula for light neutrinos $m_\nu = M_D(M_{RS}^{-1})^T M_S M_{RS}^{-1} M_D^T$ reduces to $m_\nu = \kappa_\nu M_S = (k_D^2/k_{RS}^2)$. Thus, M_S entirely dictates the physical light neutrino spectrum and the resulting structure of M_S is as follows,

$$M_S = \underbrace{\begin{pmatrix} b + \frac{2a}{3} & -\frac{a}{3} & -\frac{a}{3} \\ -\frac{a}{3} & \frac{2a}{3} & b - \frac{a}{3} \\ -\frac{a}{3} & b - \frac{a}{3} & \frac{2a}{3} \end{pmatrix}}_{M_S^{(0)}} + \underbrace{\begin{pmatrix} 0 & 0 & d \\ 0 & d & 0 \\ d & 0 & 0 \end{pmatrix}}_{M_S^{(\text{corr})}}. \quad (2.16)$$

Here, $a = \alpha_S v_S$, $b = \beta_S u$ and $d = \gamma_S u'$. In principle, a, b, d are (in general) complex parameters, but we will write them as separate moduli and phases when needed.

- **Charged Lepton mass matrix M_ℓ :** The diagonal structure of M_ℓ , from the trivial contraction of A_4 singlets without the need for additional flavons, is given by

$$M_\ell = v \text{diag}(\alpha_\ell, \beta_\ell, \gamma_\ell). \quad (2.17)$$

The values of $(\alpha_\ell, \beta_\ell, \gamma_\ell)$ are decided by the usual charged lepton Yukawa couplings (y_e, y_μ, y_τ) . Thus, the structure of charged lepton mass matrix is already diagonal predicting $U_\ell = \mathbf{I}$. This simplifies the relation $U_{\text{PMNS}} = U_\ell^\dagger U_\nu \equiv U_\nu$ and thus, the A_4 driven predictive mixing matrix for light neutrinos can be compared with the experimentally known U_{PMNS} providing important correlations between neutrino observables and input model parameters in a minimal and predictive way.

3 Predictive structure of mass matrices for double seesaw framework

In the double seesaw mechanism the neutrino mass matrices arise through the interplay between the Dirac neutrino mass matrix M_D , the mixing matrix M_{RS} connecting the right-handed neutrinos and sterile neutrinos, and the bare Majorana mass term for the sterile neutrinos M_S . The resulting double seesaw mass formula for the light neutrinos is given by

$$m_\nu = M_D(M_{RS}^{-1})^T M_S M_{RS}^{-1} M_D^T. \quad (3.1)$$

The smallness of the light neutrino Majorana mass matrix in the double seesaw mechanism, as given in Eq. (3.1), admits several possible realizations depending on the structure and relative hierarchy of the Dirac mass matrix M_D and the right-handed-sterile mixing matrix M_{RS} . In general, the suppression of light neutrino masses arises from the successive inversion of the heavy mass scales associated with M_{RS} and the sterile Majorana mass matrix M_S ,

allowing sub-eV neutrino masses even when the Dirac mass terms are of the order of the electroweak scale.

Different choices of M_D and M_{RS} —such as diagonal or non-diagonal textures, hierarchical or degenerate eigenvalues, and proportional structures motivated by flavor symmetries—lead to distinct realizations of this suppression. In particular, when M_D and M_{RS} share a common flavor structure and are proportional to each other, a screening mechanism emerges in which their flavor dependence cancels out in the effective light neutrino mass matrix. In this case, the entire flavor structure of m_ν is governed solely by the sterile-sector mass matrix M_S , while the overall neutrino mass scale is controlled by the ratio of the Dirac and intermediate mass scales. This provides a natural and symmetry-driven explanation for the smallness and simplicity of the light neutrino mass matrix in the double seesaw framework. Following Refs. [61–66], we focus in the present work on a particularly well-motivated and predictive realization in which M_D and M_{RS} share the same flavor structure.

Concretely, we consider the case in which both M_D and M_{RS} are proportional to the identity matrix,

$$M_D = k_D \mathbf{I}, \quad M_{RS} = k_{RS} \mathbf{I}, \quad (3.2)$$

where k_D and k_{RS} are real constants satisfying $|k_D| < |k_{RS}|$. In this limit one immediately obtains

$$M_D M_{RS}^{-1} = \frac{k_D}{k_{RS}} \mathbf{I}, \quad (3.3)$$

so that the ratio of the Dirac and right-handed-sterile mass matrices is flavor-universal.

Such a structure arises naturally in models with non-Abelian discrete flavor symmetries. In particular, the diagonal form of M_D follows from the flavor assignments of the left-handed lepton doublets and right-handed neutrinos, while M_{RS} acquires an identical structure due to the same symmetry constraints. More generally, the screening condition does not require M_D and M_{RS} to be strictly diagonal; it is sufficient that they be proportional to each other, even if both are non-diagonal, so that their flavor dependence cancels in the effective light neutrino mass matrix.

Indeed, assuming a proportionality relation

$$M_{RS} = \kappa M_D, \quad (3.4)$$

and substituting this into the general double seesaw formula given in Eq.(3.1), leads to a remarkable simplification. Using $M_{RS}^{-1} = \kappa^{-1} M_D^{-1}$, one finds

$$M_D M_{RS}^{-1} = \kappa^{-1} \mathbf{I}, \quad (3.5)$$

and hence

$$m_\nu = \kappa^{-2} M_S. \quad (3.6)$$

As a result, all flavor dependence associated with the Dirac and right-handed-sterile sectors cancels out, and the entire flavor structure of the light neutrino mass matrix is dictated solely by the sterile-sector Majorana mass matrix M_S . The parameters M_D and M_{RS} control only the overall mass scale through the proportionality factor κ^{-2} .

This phenomenon, commonly referred to as the *screening mechanism*, provides a natural explanation for both the smallness and the simplicity of the light neutrino mass matrix. Moreover, it enhances the predictivity of the framework, as the low-energy neutrino masses and mixing parameters can be traced directly to the flavor structure of M_S . As discussed in Refs. [28, 63], the equality and simultaneous diagonal structure of M_D and M_{RS} may arise as a consequence of residual $Z_2 \times Z_2$ symmetries [64]. With the inclusion of an additional permutation symmetry acting on the diagonal entries, one can further justify the degeneracy of their eigenvalues. Such symmetry-based realizations of the screening mechanism have been widely explored in the literature on double seesaw models [37, 61–66], and form the theoretical basis for the predictive A_4 -symmetric framework adopted in this work.

3.1 Diagonal and degenerate structure of M_D and M_{RS}

For analytic simplification for light neutrino masses and mixing within double seesaw framework, we consider the particularly simple and symmetry-motivated case in which both the Dirac mass matrix M_D and the right-handed-sterile mixing matrix M_{RS} are diagonal and degenerate. Such a structure naturally arises in the presence of A_4 flavor symmetry, as discussed in the previous subsection, and leads to a highly predictive realization of the screening mechanism. Specifically, we consider the A_4 -predicted structure of M_D and M_{RS} as follows,

$$M_D = (v \kappa_D) \mathbf{I}, \quad M_{RS} = (v_T \kappa_{RS}) \mathbf{I}, \quad (3.7)$$

where v denotes the Standard Model Higgs vacuum expectation value, v_T is the sterile-sector (triplet) vacuum expectation value of the flavon field. The other parameters κ_D and κ_{RS} are real dimensionless parameters encoding the strengths of the Dirac and right-handed-sterile interactions, respectively. We can relate neutrino mass matrix \tilde{m}_ν as follows:

Substituting these expressions into the general double seesaw formula, the effective light neutrino mass matrix takes the form

$$m_\nu = \underbrace{\left(\frac{v^2}{v_T^2} \right) \left(\frac{\kappa_D^2}{\kappa_{RS}^2} \right)}_{\equiv \kappa_\nu} M_S \equiv \kappa_\nu M_S, \quad (3.8)$$

with

$$\kappa_\nu \equiv \left(\frac{v^2}{v_T^2} \right) \left(\frac{\kappa_D^2}{\kappa_{RS}^2} \right). \quad (3.9)$$

This relation explicitly demonstrates the screening mechanism: all flavor dependence of the light neutrino mass matrix originates from the sterile-sector Majorana mass matrix M_S , while the overall neutrino mass scale is governed solely by the prefactor κ_ν . As a result, once M_S is specified, the mixing angles and CP phases are completely fixed up to an overall mass normalization, rendering the framework highly predictive.

Sterile-sector mass texture. In the present work, the sterile mass matrix M_S is chosen as

a sum of an A_4 -symmetric leading-order contribution and a symmetry-breaking correction:

$$M_S = \underbrace{\begin{pmatrix} b + \frac{2a}{3} & -\frac{a}{3} & -\frac{a}{3} \\ -\frac{a}{3} & \frac{2a}{3} & b - \frac{a}{3} \\ -\frac{a}{3} & b - \frac{a}{3} & \frac{2a}{3} \end{pmatrix}}_{M_S^{(0)}} + \underbrace{\begin{pmatrix} 0 & 0 & d \\ 0 & d & 0 \\ d & 0 & 0 \end{pmatrix}}_{M_S^{(\text{corr})}}. \quad (3.10)$$

The first term yields exact tribimaximal mixing, while the correction term breaks the symmetry in a controlled manner, generating a nonzero reactor angle and CP violation.

Step 1: Transformation to the TBM basis

Defining $\tilde{m}_\nu = m_\nu / \kappa_\nu$, the redefined neutrino mass matrix is read as

$$\tilde{m}_\nu \equiv M_S = \begin{pmatrix} b + \frac{2a}{3} & -\frac{a}{3} & -\frac{a}{3} \\ -\frac{a}{3} & \frac{2a}{3} & b - \frac{a}{3} \\ -\frac{a}{3} & b - \frac{a}{3} & \frac{2a}{3} \end{pmatrix} + \begin{pmatrix} 0 & 0 & d \\ 0 & d & 0 \\ d & 0 & 0 \end{pmatrix}. \quad (3.11)$$

The symmetric part \tilde{m}_ν is diagonalized by the tribimaximal matrix U_{TBM} . We therefore transform \tilde{m}_ν into the TBM basis,

$$\tilde{m}'_\nu = U_{\text{TBM}}^T \tilde{m}_\nu U_{\text{TBM}}. \quad (3.12)$$

where,

$$U_{\text{TBM}} = \begin{pmatrix} \sqrt{2/3} & 1/\sqrt{3} & 0 \\ -1/\sqrt{6} & 1/\sqrt{3} & -1/\sqrt{2} \\ -1/\sqrt{6} & 1/\sqrt{3} & 1/\sqrt{2} \end{pmatrix}. \quad (3.13)$$

A direct evaluation (using the well-known form of U_{TBM}) yields

$$\tilde{m}'_\nu = \begin{pmatrix} a + b - \frac{d}{2} & 0 & -\frac{\sqrt{3}}{2}d \\ 0 & b + d & 0 \\ -\frac{\sqrt{3}}{2}d & 0 & a - b + \frac{d}{2} \end{pmatrix}. \quad (3.14)$$

Thus, in the TBM basis the mass matrix is block-diagonal, with nonvanishing off-diagonal entries appearing only in the (1, 3) sector.

Step 2: Rotation in the 1–3 plane

Since the (1, 3) block is the only non-diagonal part of Eq. (3.14), the matrix can be fully diagonalized by a single unitary rotation in the 1–3 plane,

$$U_{13}(\theta, \psi) = \begin{pmatrix} \cos \theta & 0 & e^{-i\psi} \sin \theta \\ 0 & 1 & 0 \\ -e^{i\psi} \sin \theta & 0 & \cos \theta \end{pmatrix}, \quad (3.15)$$

where θ is a real mixing angle and ψ is a CP-violating phase. The diagonalization condition reads

$$U_{13}^T(\theta, \psi) \tilde{m}'_\nu U_{13}(\theta, \psi) = \text{diag}(\tilde{m}_1 e^{i\phi_1}, \tilde{m}_2 e^{i\phi_2}, \tilde{m}_3 e^{i\phi_3}), \quad (3.16)$$

where \tilde{m}_i are the (real, non-negative) eigenvalues of M_S and ϕ_i are the associated Majorana phases. Explicitly, one finds

$$\tilde{m}_1 e^{i\phi_1} = a + \sqrt{b^2 + d^2 - bd}, \quad (3.17)$$

$$\tilde{m}_2 e^{i\phi_2} = b + d, \quad (3.18)$$

$$\tilde{m}_3 e^{i\phi_3} = a - \sqrt{b^2 + d^2 - bd}. \quad (3.19)$$

Neutrino mass eigenvalues and phases

The physical light neutrino masses are related to the sterile-sector eigenvalues via the screening factor κ_ν ,

$$m_i = \kappa_\nu \tilde{m}_i = \kappa_\nu M_{S_i}, \quad (i = 1, 2, 3), \quad (3.20)$$

demonstrating that the entire neutrino mass spectrum is dictated by the flavon-induced structure of M_S .

For convenience, we introduce the dimensionless ratios

$$\lambda_1 e^{i\phi_{db}} \equiv \frac{d}{b}, \quad \lambda_2 e^{i\phi_{ab}} \equiv \frac{a}{b}, \quad b \neq 0, \quad (3.21)$$

so that $a = b \lambda_2 e^{i\phi_{ab}}$ and $d = b \lambda_1 e^{i\phi_{db}}$. In terms of these parameters, the light neutrino masses can be written as

$$m_1 e^{i\phi_1} = \kappa_\nu b \left(\lambda_2 e^{i\phi_{ab}} + \sqrt{1 + \lambda_1^2 e^{2i\phi_{db}} - \lambda_1 e^{i\phi_{db}}} \right), \quad (3.22a)$$

$$m_2 e^{i\phi_2} = \kappa_\nu b \left(1 + \lambda_1 e^{i\phi_{db}} \right), \quad (3.22b)$$

$$m_3 e^{i\phi_3} = \kappa_\nu b \left(\lambda_2 e^{i\phi_{ab}} - \sqrt{1 + \lambda_1^2 e^{2i\phi_{db}} - \lambda_1 e^{i\phi_{db}}} \right). \quad (3.22c)$$

Taking absolute values, the physical masses are

$$\begin{aligned} m_1 &= |\kappa_\nu b| \left[(\lambda_2 \cos \phi_{ab} - C)^2 + (\lambda_2 \sin \phi_{ab} - D)^2 \right]^{1/2}, \\ m_2 &= |\kappa_\nu b| \left[1 + \lambda_1^2 + 2\lambda_1 \cos \phi_{db} \right]^{1/2}, \\ m_3 &= |\kappa_\nu b| \left[(\lambda_2 \cos \phi_{ab} + C)^2 + (\lambda_2 \sin \phi_{ab} + D)^2 \right]^{1/2}, \end{aligned} \quad (3.23)$$

where

$$\begin{aligned} C &= \left[\frac{A + \sqrt{A^2 + B^2}}{2} \right]^{1/2}, & D &= \left[\frac{-A + \sqrt{A^2 + B^2}}{2} \right]^{1/2}, \\ A &= 1 + \lambda_1^2 \cos 2\phi_{db} - \lambda_1 \cos \phi_{db}, & B &= \lambda_1^2 \sin 2\phi_{db} - \lambda_1 \sin \phi_{db}. \end{aligned} \quad (3.24)$$

The corresponding Majorana phases are given by

$$\begin{aligned} \phi_1 &= \tan^{-1} \left(\frac{\lambda_2 \sin \phi_{ab} - D}{\lambda_2 \cos \phi_{ab} - C} \right), \\ \phi_2 &= \tan^{-1} \left(\frac{\lambda_1 \sin \phi_{db}}{1 + \lambda_1 \cos \phi_{db}} \right), \\ \phi_3 &= \tan^{-1} \left(\frac{\lambda_2 \sin \phi_{ab} + D}{\lambda_2 \cos \phi_{ab} + C} \right). \end{aligned} \quad (3.25)$$

3.1.1 Mass spectra and normalization

Let us denote by M_{S_i} ($i = 1, 2, 3$) the eigenvalues of the dimensionless sterile-sector mass matrix $\tilde{m}_\nu \equiv M_S$, which encodes the full flavor structure of the theory after screening. Owing to the proportionality $m_\nu = \kappa_\nu M_S$, the physical light neutrino masses are simply given by

$$m_i = \kappa_\nu M_{S_i}, \quad (3.26)$$

where the factor κ_ν controls the overall mass scale, while the mass ratios and mixing structure are entirely determined by the A_4 -driven texture of M_S .

The normalization factor κ_ν is fixed by requiring consistency with the experimentally measured atmospheric mass-squared splitting. For normal mass ordering (NO), this yields

$$\kappa_\nu^2 = \frac{|\Delta m_{\text{atm}}^2|}{M_{S_3}^2 - M_{S_1}^2}, \quad (3.27)$$

$$\Delta m_{21}^2 = \kappa_\nu^2 (M_{S_2}^2 - M_{S_1}^2), \quad (3.28)$$

so that, once κ_ν is determined from the atmospheric scale, the solar mass-squared difference follows as a prediction of the model. This feature highlights the predictive power of the screening mechanism: only one mass scale is fixed by data, while the remaining mass splitting is governed by the structure of M_S .

Heavy neutrino spectrum in the double seesaw. Within the A_4 -symmetric construction considered here, the Dirac and right-handed-sterile mass matrices are proportional to the identity. As a result, the effective right-handed neutrino (RHN) mass matrix obtained after integrating out the sterile states takes the simple form

$$M_R = -M_{RS} M_S^{-1} M_{RS}^T = -v_T^2 k_{RS}^2 M_S^{-1}. \quad (3.29)$$

Since the sterile-sector mass matrix M_S is diagonalized by the same unitary matrix as the light neutrino mass matrix,

$$U_S \equiv U_\nu = U_{\text{TBM}} U_{13} U_m, \quad (3.30)$$

it follows that the RHN mass matrix is diagonalized by $U_R = U_\nu^*$. The eigenvalues of M_R are therefore inversely proportional to those of M_S .

Using the relation $M_{S_j} = m_j / \kappa_\nu$, the RHN masses can be written as

$$M_{R_j} = \frac{v_T^2 k_{RS}^2}{M_{S_j}} = \frac{v_T^2 k_{RS}^2}{(m_j / \kappa_\nu)} = \frac{v^2 k_D^2}{m_j}, \quad (j = 1, 2, 3). \quad (3.31)$$

This inverse scaling between light and heavy neutrino masses is a characteristic hallmark of the double seesaw mechanism and arises naturally once screening is realized through the proportionality of M_D and M_{RS} .

Implications for leptogenesis. The hierarchical structure implied by $M_{R_j} \propto 1/m_j$ has important phenomenological consequences. In particular, the scale and ordering of the RHN masses are directly correlated with the low-energy neutrino spectrum, providing a natural

setting for thermal leptogenesis [38, 39, 67–71]. The same A_4 -induced structure that controls neutrino mixing at low energies thus also governs the properties of the heavy states responsible for generating the observed matter–antimatter asymmetry of the Universe. A detailed analysis of leptogenesis within the double seesaw framework implemented with A_4 flavor symmetry is beyond the scope of the present work and will be presented separately.

4 Mixing Structure from A_4 : Tribimaximal Form and a Single Complex Rotation

The double seesaw–invoked A_4 framework exhibits a highly constrained and predictive flavor structure for neutrino mixing. At leading order, the sterile-sector Majorana mass matrix respects the A_4 symmetry and gives rise to the well-known tribimaximal (TBM) mixing pattern. Deviations from exact TBM originate from controlled A_4 -breaking effects in the sterile sector, which are essential for generating a nonzero reactor mixing angle and leptonic CP violation in agreement with experimental observations. Working in the TBM basis, the corrected light neutrino mass matrix develops nonvanishing off-diagonal entries only in the 1–3 sector. Consequently, the full diagonalization of the neutrino mass matrix requires a single complex rotation in this plane. The neutrino diagonalization matrix can therefore be written as

$$U_\nu = U_{\text{TBM}} U_{13}(\theta, \psi) U_m, \quad (4.1)$$

where $U_{13}(\theta, \psi)$ denotes a unitary rotation in the 1–3 plane characterized by a real angle θ and a phase ψ . The diagonal phase matrix

$$U_m = \text{diag}(1, e^{i\alpha}, e^{i\beta}) \quad (4.2)$$

contains the physical Majorana phases associated with the light neutrino mass eigenstates.

PMNS matrix and charged-lepton sector. The leptonic mixing matrix is defined as

$$U_{\text{PMNS}} = U_\ell^\dagger U_\nu, \quad (4.3)$$

where U_ℓ and U_ν diagonalize the charged-lepton and neutrino mass matrices, respectively. In the present A_4 realization, the charged-lepton mass matrix is diagonal, implying

$$U_\ell = \mathbf{I}, \quad (4.4)$$

and hence

$$U_{\text{PMNS}} = U_\nu. \quad (4.5)$$

The leptonic mixing matrix therefore inherits the TBM structure at leading order, corrected by a single complex 1–3 rotation and a diagonal Majorana phase matrix.

Additionally, the PMNS matrix can be expressed in the standard PDG parameterization as

$$U_{\text{PMNS}} = \begin{pmatrix} c_{12}c_{13} & s_{12}c_{13} & s_{13}e^{-i\delta_{\text{CP}}} \\ -c_{23}s_{12} - c_{12}s_{13}s_{23}e^{i\delta_{\text{CP}}} & c_{12}c_{23} - s_{12}s_{13}s_{23}e^{i\delta_{\text{CP}}} & s_{23}c_{13} \\ s_{12}s_{23} - c_{12}c_{23}s_{13}e^{i\delta_{\text{CP}}} & -c_{12}s_{23} - s_{12}s_{13}c_{23}e^{i\delta_{\text{CP}}} & c_{23}s_{13} \end{pmatrix} U_m \quad (4.6)$$

where $(c_\alpha, s_\alpha) \equiv (\cos \theta_\alpha, \sin \theta_\alpha)$. Equating Eqs. (4.1) and (4.6) establishes a direct mapping between the model parameters (θ, ψ) and the observable mixing angles and CP-violating phase.

Mixing angles. By comparing the relevant matrix elements, the solar mixing angle is obtained from the $(1, 2)$ element as

$$\sin \theta_{12} = \frac{1}{\sqrt{3} \cos \theta_{13}}, \quad (4.7)$$

while the reactor mixing angle yields by equating the $(1, 3)$ elements

$$\sin \theta_{13} = \sqrt{\frac{2}{3}} |\sin \theta|, \quad (4.8)$$

Furthermore, the atmospheric mixing angle follows from the ratio of the $(2, 3)$ and $(3, 3)$ elements,

$$\tan \theta_{23} = \frac{e^{-i\psi} \sin \theta + \sqrt{3} \cos \theta}{e^{-i\psi} \sin \theta - \sqrt{3} \cos \theta}. \quad (4.9)$$

This demonstrates that the reactor mixing angle originates entirely from the single 1–3 rotation induced by A_4 -breaking effects in the sterile sector.

Phase structure and Dirac CP violation. The Majorana phases are parameterized as

$$\phi_1 = 2\pi, \quad \phi_2 = 2\pi - \alpha, \quad \phi_3 = 2\pi - \beta, \quad (4.10)$$

with $\alpha, \beta \in [0, 2\pi]$. The phase ψ associated with the 1–3 rotation directly controls leptonic CP violation and is identified with the Dirac CP phase as

$$\delta_{\text{CP}} = \begin{cases} \psi, & \sin \theta > 0, \\ \psi \pm \pi, & \sin \theta < 0, \end{cases} \quad (4.11)$$

up to a discrete sign convention. Consequently, in the double seesaw-invoked A_4 framework, all three mixing angles and the Dirac CP-violating phase are determined by only two parameters (θ, ψ) , originating from the controlled breaking of A_4 symmetry in the sterile sector. This minimal structure naturally accommodates the observed pattern of neutrino mixing and CP violation while retaining a high degree of predictivity. Using the NuFIT 6.0 3σ allowed range for the reactor mixing angle, $\theta_{13} \in [8.18^\circ, 8.87^\circ]$, which implies $\sin \theta_{13} > 0$ throughout the interval, we obtain from Eq. (4.8) the corresponding range

$$\sin \theta \in [0.174, 0.188],$$

thereby fixing $\sin \theta > 0$ for all viable solutions. As a consequence, the Dirac CP-violating phase is unambiguously identified with the phase ψ associated with the single 1–3 rotation, leading to

$$\boxed{\delta_{\text{CP}} = \psi} \quad (4.12)$$

in the degenerate Yukawa coupling limit of the model.

Furthermore, since $\tan \psi = \tan \delta_{\text{CP}}$ irrespective of the discrete ambiguity $\delta_{\text{CP}} = \psi$ or $\psi \pm \pi$, the Dirac CP phase can be expressed directly in terms of the underlying sterile-sector phases. Using the analytic relations derived from the A_4 -symmetric mass texture, we obtain

$$\boxed{\tan \delta_{\text{CP}} = -\frac{\sin \phi_{db}}{\lambda_2 \cos(\phi_{ab} - \phi_{db})}} \quad (4.13)$$

which establishes a transparent connection between low-energy CP violation and the high-scale parameters ϕ_{ab} , ϕ_{db} , and λ_2 of the sterile sector. This relation highlights the predictive power of the double seesaw-invoked A_4 framework, in which the observed Dirac CP phase is not a free parameter but is dynamically determined by the flavor structure of the heavy neutrino sector.

4.1 Diagonalization of the 1–3 Block and Physical Parameterization

To make the physical origin of lepton mixing and CP violation explicit, it is convenient to reparametrize the complex parameters of the effective neutrino mass matrix in terms of dimensionless ratios. We define

$$\frac{a}{b} = \lambda_2 e^{i\phi_{ab}}, \quad \frac{d}{b} = \lambda_1 e^{i\phi_{db}}, \quad (4.14)$$

where a , b , and d are the complex parameters appearing in the neutrino mass matrix after the double seesaw mechanism. Without loss of generality, b is chosen to be real and positive, so that all physical phases reside in the phase differences ϕ_{ab} and ϕ_{db} . Here

$$\lambda_1 \equiv \left| \frac{d}{b} \right|, \quad \lambda_2 \equiv \left| \frac{a}{b} \right|$$

denote the magnitudes of the ratios, while $\phi_{ab} \equiv \arg(a/b)$ and $\phi_{db} \equiv \arg(d/b)$ encode the CP-violating phases. Since an overall rescaling of the mass matrix does not affect mixing observables, these ratios constitute the fundamental parameters controlling neutrino mixing and CP violation in the model. In the tribimaximal basis, the effective light neutrino mass matrix develops a nontrivial structure only in the 1–3 subspace. This block can be diagonalized by a unitary rotation characterized by a real mixing angle θ and a CP-violating phase ψ . Requiring the off-diagonal elements of the 1–3 block to vanish yields the analytic expression

$$\tan 2\theta = \frac{\sqrt{3} \lambda_1 \cos \phi_{db}}{\lambda_1 \cos \psi \cos \phi_{db} - 2(\lambda_2 \sin \psi \sin \phi_{ab} + \cos \psi)}, \quad (4.15)$$

where the factor of $\sqrt{3}$ originates from the underlying A_4 group-theoretical structure of the mass matrix. The phase ψ is fixed by the requirement that the diagonalized neutrino mass eigenvalues be real and positive. This condition uniquely determines ψ as

$$\tan \psi = -\frac{\sin \phi_{db}}{\lambda_2 \cos(\phi_{ab} - \phi_{db})}. \quad (4.16)$$

Equation (4.16) explicitly shows that leptonic CP violation arises from the relative phase between the sterile-sector parameters a and d . In the CP-conserving limit $\phi_{db} \rightarrow 0$, the phase ψ vanishes and the neutrino mixing matrix becomes real. Equations (4.15) and (4.16) demonstrate that both lepton mixing and CP violation are governed by the dimensionless ratios $\lambda_1 = d/b$ and $\lambda_2 = a/b$ and their associated phases, rather than by arbitrary Yukawa couplings. Once these quantities are fixed, the mixing angle θ , the CP phase ψ , and consequently all physical PMNS parameters are fully determined.

4.2 Special Limits and Physical Interpretation

Several limiting cases of the parameter space provide valuable insight into the origin of neutrino mixing and leptonic CP violation within the double seesaw–invoked A_4 framework.

CP-conserving limit. If the relative phase satisfies

$$\sin \phi_{db} = 0 \quad (\phi_{db} = 0, \pi), \quad (4.17)$$

the ratio d/b becomes purely real. In this case, Eq. (4.16) implies $\psi = 0$ or π , and the leptonic mixing matrix contains no irreducible complex phase. Consequently, the Jarlskog invariant vanishes,

$$J_{\text{CP}} = 0, \quad (4.18)$$

indicating the absence of Dirac-type leptonic CP violation. This demonstrates that CP violation in the present framework originates entirely from the relative complex phase among the double seesaw parameters.

Tribimaximal mixing limit. In the limit

$$\lambda_1 = \left| \frac{d}{b} \right| \rightarrow 0 \quad (d \rightarrow 0), \quad (4.19)$$

the double seesaw correction disappears and the effective light neutrino mass matrix reduces to its leading-order A_4 -symmetric form. The neutrino mixing is then exactly tribimaximal, yielding

$$\theta_{13} \rightarrow 0, \quad \theta_{12} = 35.3^\circ, \quad \theta_{23} = 45^\circ. \quad (4.20)$$

This limit clearly identifies the parameter d as the sole source of deviation from exact tribimaximal mixing in the present construction.

Realistic mixing and leptonic CP violation. For nonzero λ_1 and a genuinely complex phase ϕ_{db} , the 1–3 block acquires a complex off-diagonal structure. This induces a nonvanishing rotation angle θ and phase ψ , leading simultaneously to a nonzero reactor angle θ_{13} and potentially large Dirac CP violation. Importantly, both effects originate from the same source—the magnitude and phase of the double seesaw correction—yielding a strong correlation between θ_{13} and δ_{CP} . This unified origin naturally explains the observed deviation from tribimaximal mixing and allows for sizable leptonic CP violation without fine-tuning, rendering the framework both predictive and phenomenologically viable.

4.3 Derivation of Double Seesaw Neutrino Masses in the Degenerate Yukawa Limit

In this subsection, we derive the light neutrino mass spectrum and its parametric structure arising from the double seesaw mechanism in the limit of degenerate Yukawa couplings. Owing to the hierarchical suppression involving the Dirac, right-handed, and sterile fermion sectors, the double seesaw framework naturally generates sub-eV neutrino masses without requiring fine-tuning of Yukawa couplings. After integrating out the heavy states, the effective light neutrino mass matrix M_ν depends on three complex parameters a , b , and d , which originate from the A_4 -symmetric sterile-sector Majorana mass matrix and its controlled breaking. In the degenerate Yukawa limit, the overall mass scale factorizes and can be expressed in terms of a single effective parameter,

$$\kappa_\nu \equiv \left(\frac{v^2}{v_T^2} \right) \left(\frac{\kappa_D^2}{\kappa_{RS}^2} \right), \quad (4.21)$$

where v is the Standard Model Higgs vacuum expectation value, v_T denotes the sterile-sector vacuum expectation value, and κ_D and κ_{RS} parametrize the strengths of the Dirac and right-handed-sterile couplings, respectively. Diagonalizing the effective light neutrino mass matrix, the mass eigenvalues are obtained as

$$\begin{aligned} m_1 &= \kappa_\nu \left[a - \sqrt{b^2 - bd + d^2} \right], \\ m_2 &= \kappa_\nu (b + d), \\ m_3 &= \kappa_\nu \left[a + \sqrt{b^2 - bd + d^2} \right], \end{aligned} \quad (4.22)$$

where the square-root structure reflects the mixing between the parameters b and d induced by the off-diagonal structure of the sterile-sector mass matrix. To further streamline the analytic structure, we define the simplified combinations

$$p \equiv \frac{m_1}{\kappa_\nu}, \quad q \equiv \frac{m_2}{\kappa_\nu}, \quad r \equiv \frac{m_3}{\kappa_\nu}. \quad (4.23)$$

In terms of these variables, the relations in Eq. (4.22) take the compact form

$$p = a - \sqrt{b^2 - bd + d^2}, \quad q = b + d, \quad r = a + \sqrt{b^2 - bd + d^2}. \quad (4.24)$$

These expressions can be inverted to express the underlying model parameters directly in terms of the physical neutrino masses,

$$a = \frac{p+r}{2}, \quad b = \frac{q}{2} + \frac{1}{2} \sqrt{\frac{(r-p)^2}{3} - \frac{q^2}{3}}, \quad d = \frac{q}{2} - \frac{1}{2} \sqrt{\frac{(r-p)^2}{3} - \frac{q^2}{3}}. \quad (4.25)$$

This parametrization is particularly well suited for numerical analyses, as it establishes a direct and transparent mapping between the experimentally measured light neutrino masses and the underlying parameters of the A_4 -symmetric double seesaw framework. All dependence on the heavy-sector scales is encoded in the single parameter κ_ν , while the flavor

structure and mass splittings are governed solely by the parameters a , b , and d . In the following section, we will perform a comprehensive numerical scan over the underlying model parameters (a, b, d, κ_ν) , subject to current experimental constraints on neutrino oscillation observables. By examining the resulting predictions for neutrino masses, mixing angles, and CP-violating phases with global-fit data and the recent high-precision JUNO measurements, we identify the phenomenologically viable regions of the parameter space and extract representative benchmark points.

5 Numerical Analysis and Constraints on Model Parameters

In this section, we intend to perform a detailed numerical analysis of the neutrino masses and neutrino mixing angles as predicted by the double seesaw mechanism embedded within the A_4 flavor-symmetric framework. Building upon the analytical diagonalization conditions established in the previous sections, we show that the structure of the effective light neutrino mass matrix m_ν is mostly dictated by the diagonalization of the sterile-sector Majorana mass matrix M_S , whose A_4 -invariant form plays a central role in determining the low-energy neutrino phenomenology. By performing a comprehensive scan over the fundamental model parameters and imposing the current 3σ constraints from global neutrino oscillation data, we systematically explore both normal and inverted neutrino mass orderings. This procedure allows us to delineate the phenomenologically viable regions of parameter space, identify representative benchmark points, and uncover characteristic correlations among neutrino masses, mixing angles, and CP-violating phases that emerge as distinctive signatures of the double seesaw realization of A_4 symmetry.

5.1 For Normal Ordering

The sterile-sector Majorana mass matrix M_S , constrained by the underlying A_4 symmetry, is parameterized by three independent complex quantities a , b , and d . The absolute values of these parameters are scanned over the ranges:

$$\begin{aligned} |a| &\in [4.6 \times 10^9, 3.26 \times 10^{13}] \text{ eV}, \\ |b| &\in [3.04 \times 10^9, 9.40 \times 10^{12}] \text{ eV}, \\ |d| &\in [9.35 \times 10^8, 3.26 \times 10^{13}] \text{ eV}, \end{aligned} \tag{5.1}$$

while their phases are varied freely. These ranges are chosen such that the resulting low-energy neutrino observables lie within the 3σ allowed regions of the NuFIT 6.0 global analysis. The Yukawa-sector parameters are simultaneously scanned within $k_{RS} \in [0.99, 1.0]$ and $k_D \in [1 \times 10^{-7}, 4 \times 10^{-7}]$, ensuring perturbativity and consistency with the hierarchical structure required by the double seesaw mechanism. The Standard Model Higgs VEV is taken as $v = 174$ GeV while v_T (contributing to the mass M_{RS}) is fixed at 10 TeV around which we assign VEVs to flavon fields.

For each randomly generated parameter set, the effective light neutrino mass matrix m_ν is constructed and diagonalized numerically. Assuming normal mass ordering, the light neutrino masses are obtained in the ranges

$$\begin{aligned} m_1 &\in [4.0 \times 10^{-4}, 3.99 \times 10^{-3}] \text{ eV}, \\ m_2 &\in [8.33 \times 10^{-3}, 9.82 \times 10^{-3}] \text{ eV}, \\ m_3 &\in [4.96 \times 10^{-2}, 5.12 \times 10^{-2}] \text{ eV}, \end{aligned} \quad (5.2)$$

which correctly reproduce the observed solar and atmospheric mass-squared differences,

$$\begin{aligned} \Delta m_{21}^2 &\in [6.92, 8.05] \times 10^{-5} \text{ eV}^2, \\ \Delta m_{31}^2 &\in [2.46, 2.61] \times 10^{-3} \text{ eV}^2, \end{aligned} \quad (5.3)$$

in excellent agreement with current oscillation data.

The corresponding leptonic mixing angles extracted from the diagonalization of m_ν are found to lie within

$$\begin{aligned} \theta_{12} &\in [35.68^\circ, 35.75^\circ], \\ \theta_{13} &\in [8.18^\circ, 8.87^\circ], \\ \theta_{23} &\in [45.00^\circ, 51.33^\circ], \end{aligned} \quad (5.4)$$

exhibiting a clear preference for the higher-octant solution of θ_{23} . The Dirac CP-violating phase is constrained to

$$\delta_{CP} \equiv \psi \in [-90^\circ, 90^\circ], \quad (5.5)$$

reflecting the restricted phase structure imposed by the A_4 symmetry.

A comprehensive summary of the allowed model parameters and neutrino observables within the 3σ region for normal ordering is presented in Table 2, highlighting the highly constrained nature of the viable parameter space and the strong correlations among neutrino masses, mixing angles, and the underlying model parameters.

Benchmark Point and Matrix Structure: To illustrate the structure of the model, we present a representative benchmark point. For this point, the Dirac and intermediate mass matrices are

$$M_D = v k_D \mathbf{I} = 6.9 \times 10^4 \mathbf{I} \text{ eV}, \quad (5.6)$$

$$M_{RS} = v_T k_{RS} \mathbf{I} = 9.95 \times 10^{12} \mathbf{I} \text{ eV}. \quad (5.7)$$

The sterile-sector Majorana mass matrix takes the form

$$M_S = \begin{pmatrix} 7.43 & -1.85 & -3.73 \\ -1.85 & 1.83 & 1.87 \\ -3.73 & 1.87 & 3.71 \end{pmatrix} \times 10^{14} \text{ eV}, \quad (5.8)$$

leading to the effective light neutrino mass matrix

$$m_\nu = \begin{pmatrix} 0.0357 & -0.0089 & -0.0179 \\ -0.0089 & 0.0088 & 0.0090 \\ -0.0179 & 0.0090 & 0.0178 \end{pmatrix} \text{ eV}. \quad (5.9)$$

This matrix is diagonalized by a unitary transformation, yielding eigenvalues and mixing parameters consistent with current experimental constraints. The restricted structure of m_ν highlights the predictive nature of the double seesaw–invoked A_4 framework and sets the stage for the phenomenological discussions presented in the next section.

One of the salient predictions of the double-seesaw realization of the A_4 flavor framework is the emergence of large Majorana masses for the right-handed neutrinos. Such heavy states inherently violate lepton number and can therefore give rise to distinctive experimental signatures, including lepton-number-violating processes, neutrinoless double-beta decay, and possible collider observables, provided that the right-handed neutrino mass scale lies within the sensitivity reach of current or future experiments. In the present numerical analysis, we explicitly evaluate the right-handed neutrino mass matrix and the corresponding unitary matrix that diagonalizes it, which are given by

$$M_R = \begin{pmatrix} 2.688 \times 10^{11} & -6.964 \times 10^9 & 2.737 \times 10^{11} \\ -6.964 \times 10^9 & 1.107 \times 10^{12} & -5.646 \times 10^{11} \\ 2.737 \times 10^{11} & -5.646 \times 10^{11} & 8.264 \times 10^{11} \end{pmatrix} \text{ eV}, \quad (5.10)$$

$$U_R = \begin{pmatrix} 0.8035 & 0.517 + 0.256i & -0.099 + 0.010i \\ -0.324 + 0.098i & 0.517 + 0.256i & -0.052 + 0.740i \\ -0.479 - 0.098i & 0.517 + 0.256i & 0.151 - 0.635i \end{pmatrix}. \quad (5.11)$$

Table 2 presents the complete set of neutrino oscillation observables and underlying model

Table 2: Allowed ranges of model parameters and neutrino observables for normal mass ordering obtained within the double seesaw–invoked A_4 framework.

Parameter	3 σ Range	Parameter	3 σ Range
m_1 (eV)	$[4.0 \times 10^{-4}, 3.99 \times 10^{-3}]$	θ	$[10.03^\circ, 10.88^\circ]$
m_2 (eV)	$[8.329 \times 10^{-3}, 9.82 \times 10^{-3}]$	$\delta_{\text{CP}}(\psi)$	$[-89.99^\circ, 89.99^\circ]$
m_3 (eV)	$[4.96 \times 10^{-2}, 5.12 \times 10^{-2}]$	ϕ_{db}	$[0.0004^\circ, 360^\circ]$
Δm_{21}^2 (eV 2)	$[6.92 \times 10^{-5}, 8.05 \times 10^{-5}]$	ϕ_{ab}	$[0.0039^\circ, 359.999^\circ]$
Δm_{31}^2 (eV 2)	$[2.463 \times 10^{-3}, 2.606 \times 10^{-3}]$	λ_1	$[-0.55, -0.45]$
k_{RS}	$[0.99, 1.00]$	λ_2	$[1.355, 1.534]$
k_D	$[1.00 \times 10^{-7}, 3.99 \times 10^{-7}]$	M_{R_1} (GeV)	$[5.93, 97.5]$
a (GeV)	$[5.119 \times 10^5, 8.986 \times 10^6]$	M_{R_2} (GeV)	$[31.1, 580]$
b (GeV)	$[3.594 \times 10^5, 6.13 \times 10^6]$	M_{R_3} (GeV)	$[76.2, 1.20 \times 10^4]$
d (GeV)	$[-3.325 \times 10^6, -1.646 \times 10^5]$	M_{S_1} (GeV)	$[8.30 \times 10^3, 1.30 \times 10^6]$
θ_{13}	$[8.18^\circ, 8.87^\circ]$	M_{S_2} (GeV)	$[1.70 \times 10^5, 3.17 \times 10^6]$
θ_{12}	$[35.68^\circ, 35.75^\circ]$	M_{S_3} (GeV)	$[1.00 \times 10^6, 1.68 \times 10^7]$
θ_{23}	$[45.00^\circ, 51.33^\circ]$	k	$[1.42 \times 10^8, 5.74 \times 10^8]$
M_D (GeV)	$[1.74 \times 10^{-5}, 6.96 \times 10^{-5}]$	M_{RS} (GeV)	$[9.9 \times 10^3, 1.0 \times 10^4]$

parameters obtained from the numerical scan for the normal mass ordering within the double-seesaw-invoked A_4 framework. The quoted intervals correspond to the 3σ allowed regions after imposing the NuFIT 6.0 constraints on the leptonic mixing angles and neutrino mass-squared differences. Owing to the A_4 -symmetric structure of the sterile-sector Majorana mass matrix M_S , together with the degenerate forms of the Dirac mass matrix M_D and the right-handed mass matrix M_{RS} , the effective light neutrino mass matrix m_ν acquires a highly constrained texture. This results in sharply restricted predictions for the solar and atmospheric mixing angles. In particular, the model yields a narrow allowed range for θ_{12} and favors the atmospheric mixing angle θ_{23} in the higher octant, $\theta_{23} > 45^\circ$, for normal ordering. The resulting light neutrino masses (m_1, m_2, m_3) naturally reproduce the observed mass hierarchy and generate mass-squared differences Δm_{21}^2 and Δm_{31}^2 in excellent agreement with current global-fit data, including the recent high-precision determination of Δm_{21}^2 by JUNO. The allowed ranges of the CP-violating phases $(\delta_{CP}, \phi_{ab}, \phi_{db})$ and the dimensionless parameters (λ_1, λ_2) encode the residual freedom in the sterile sector, while maintaining strong correlations with low-energy neutrino observables. Overall, Table 2 demonstrates that the double-seesaw-invoked A_4 framework successfully accommodates present oscillation data for normal ordering and exhibits a high degree of predictivity, making it well suited for further scrutiny at upcoming precision neutrino experiments.

5.2 For Inverted Ordering

We now turn to study the case of inverted mass ordering (IO). In this scenario, the model parameters entering the sterile-sector Majorana mass matrix M_S are varied within the ranges

$$\begin{aligned} a &\in [2.54 \times 10^{14}, 4.46 \times 10^{15}] \text{ eV}, \\ b &\in [2.486 \times 10^{14}, 4.38 \times 10^{15}] \text{ eV}, \\ |d| &\in [2.32 \times 10^{14}, 4.18 \times 10^{15}] \text{ eV}. \end{aligned} \quad (5.12)$$

The remaining parameters associated with the Dirac and intermediate mass matrices are fixed as $v = 174$ GeV, $v_T = 10$ TeV, $k_D \in [0.99, 1.00]$, and $k_{RS} \in [1.0 \times 10^{-7}, 4.0 \times 10^{-7}]$. These choices ensure the validity of the double seesaw hierarchy and compatibility with the NuFIT 6.0 oscillation constraints.

A representative benchmark point illustrating the matrix structures in the inverted ordering case is given by

$$M_D = v k_D \mathbf{I} = 4.8 \times 10^4 \mathbf{I} \text{ eV}, \quad (5.13)$$

$$M_{RS} = v_T k_{RS} \mathbf{I} = 9.92 \times 10^{12} \mathbf{I} \text{ eV}. \quad (5.14)$$

The sterile-sector Majorana mass matrix, consistent with the A_4 flavor symmetry, takes the form

$$M_S = \begin{pmatrix} 9.040 & -1.787 & 3.199 \\ -1.787 & 8.562 & 3.677 \\ 3.199 & 3.677 & 3.575 \end{pmatrix} \times 10^{14} \text{ eV}. \quad (5.15)$$

The effective light neutrino mass matrix is obtained as

$$m_\nu = \begin{pmatrix} 0.0214 & -0.0042 & 0.0075 \\ -0.0042 & 0.0200 & 0.0087 \\ 0.0075 & 0.0087 & 0.0084 \end{pmatrix} \text{ eV.} \quad (5.16)$$

Diagonalization of the effective light neutrino mass matrix in the inverted mass ordering resulting in a spectrum with a quasi-degenerate pair (m_1, m_2) and a comparatively lighter third state m_3 , fully consistent with the 3σ ranges of the NuFIT 6.0 global analysis. As in the normal ordering case, the inverted hierarchy exhibits strong correlations among neutrino masses, mixing angles, and CP-violating phases, arising from the constrained structure imposed by the double seesaw-invoked A_4 symmetry. While these features are implicit in the mass matrices, their phenomenological implications are most transparently revealed through correlation plots. We therefore present a detailed graphical analysis in the following section to highlight the interplay between low-energy neutrino observables and underlying high-scale model parameters, enabling a clearer assessment of the model's predictivity and its sensitivity to future precision measurements.

Table 3: Allowed ranges of model parameters and neutrino observables for inverted mass ordering obtained within the double seesaw-invoked A_4 framework.

Parameter	3σ Range	Parameter	3σ Range
m_1 (eV)	$[4.85 \times 10^{-2}, 5.03 \times 10^{-2}]$	θ	$[10.10^\circ, 10.93^\circ]$
m_2 (eV)	$[4.93 \times 10^{-2}, 5.09 \times 10^{-2}]$	$\delta_{\text{CP}}(\psi)$	$[-89.99^\circ, 89.99^\circ]$
m_3 (eV)	$[4.0 \times 10^{-4}, 4.0 \times 10^{-3}]$	ϕ_{db}	$[0.0038^\circ, 359.99^\circ]$
Δm_{21}^2 (eV 2)	$[6.92 \times 10^{-5}, 8.05 \times 10^{-5}]$	ϕ_{ab}	$[0.00065^\circ, 359.99^\circ]$
Δm_{32}^2 (eV 2)	$[-2.58 \times 10^{-3}, -2.43 \times 10^{-3}]$	λ_1	$[0.859, 1.000]$
k_{RS}	$[0.99, 1.00]$	λ_2	$[0.953, 1.076]$
k_D	$[1.00 \times 10^{-7}, 3.99 \times 10^{-7}]$	M_{R_1} (GeV)	$[11.9, 195]$
a (GeV)	$[2.54 \times 10^5, 4.46 \times 10^6]$	M_{R_2} (GeV)	$[12.1, 1990]$
b (GeV)	$[2.486 \times 10^5, 4.38 \times 10^6]$	M_{R_3} (GeV)	$[153, 2.41 \times 10^4]$
d (GeV)	$[2.32 \times 10^5, 4.18 \times 10^6]$	M_{S_1} (GeV)	$[4.11 \times 10^3, 6.46 \times 10^5]$
θ_{13}	$[8.24^\circ, 8.90^\circ]$	M_{S_2} (GeV)	$[4.93 \times 10^5, 8.21 \times 10^6]$
θ_{12}	$[35.68^\circ, 35.76^\circ]$	M_{S_3} (GeV)	$[5.02 \times 10^5, 8.34 \times 10^6]$
θ_{23}	$[45.00^\circ, 51.36^\circ]$	k	$[1.42 \times 10^8, 5.74 \times 10^8]$
M_D (eV)	$[1.74 \times 10^4, 6.96 \times 10^4]$	M_{RS} (GeV)	$[9.9 \times 10^3, 1.0 \times 10^4]$

Table 3 summarizes the neutrino oscillation observables and the corresponding model parameters obtained from the numerical scan assuming inverted mass ordering within the double seesaw-invoked A_4 framework. The quoted intervals represent the 3σ allowed ranges after enforcing the NuFIT 6.0 constraints on the leptonic mixing angles and mass-squared differences. In the inverted ordering scenario, the model generically yields a quasi-degenerate

pair of heavier neutrino masses, m_1 and m_2 , while the lightest state m_3 is predicted to lie in the sub-meV to few-meV range. The experimentally measured solar and atmospheric mass-squared differences, Δm_{21}^2 and Δm_{32}^2 , are successfully reproduced within their respective allowed regions. Owing to the A_4 -symmetric structure of the sterile-sector Majorana mass matrix M_S , the leptonic mixing angles are tightly constrained. In particular, the atmospheric mixing angle θ_{23} predominantly resides in the higher octant, consistent with the normal ordering case, while the Dirac CP-violating phase δ_{CP} occupies a restricted region that exhibits a strong correlation with the internal phases ϕ_{ab} and ϕ_{db} . Furthermore, the allowed ranges of the right-handed neutrino masses M_{R_i} and sterile fermion masses M_{S_i} clearly reflect the hierarchical pattern inherent to the double seesaw mechanism. Overall, the results presented in Table 3 demonstrate that the inverted mass ordering is consistently accommodated within the double seesaw-invoked A_4 framework, while preserving non-trivial correlations among low-energy neutrino observables and high-scale model parameters.

In the case of inverted mass ordering, the double seesaw-invoked A_4 framework similarly predicts heavy Majorana masses for the right-handed neutrinos, with a structured mass spectrum governed by the sterile-sector parameters. The resulting right-handed neutrino mass matrix and its corresponding unitary diagonalization matrix reflect the underlying A_4 symmetry and exhibit characteristic correlations that can potentially give rise to lepton-number-violating signatures and collider-accessible phenomena. The explicit forms of M_R and U_R for a representative benchmark point are presented below.

$$M_R = \begin{pmatrix} 1.259 \times 10^{12} & 1.338 \times 10^{12} & -2.503 \times 10^{12} \\ 1.338 \times 10^{12} & 1.627 \times 10^{12} & -2.871 \times 10^{12} \\ -2.503 \times 10^{12} & -2.871 \times 10^{12} & 5.468 \times 10^{12} \end{pmatrix} \text{ eV},$$

$$U_R = \begin{pmatrix} 0.802 & 0.105 + 0.567i & -0.048 + 0.141i \\ -0.308 + 0.090i & 0.104 + 0.567i & -0.274 - 0.698i \\ -0.494 - 0.090i & -0.104 - 0.567i & 0.322 + 0.556i \end{pmatrix}. \quad (5.17)$$

Using the analytical expressions given in Eqs. (4.7) and (4.9), we predict the allowed ranges of the neutrino oscillation mixing angles θ_{12} and θ_{23} within our model. To examine these predictions with experimental data, we take the 3σ range of θ_{13} from the NuFIT 6.0 global analysis [72] as an additional input parameter. As summarized in Tables 3 and 4, the solar mixing angle θ_{12} is predicted to lie within a remarkably narrow interval, $\theta_{12} \in [35.68^\circ, 35.75^\circ]$ for normal ordering and $\theta_{12} \in [35.68^\circ, 35.76^\circ]$ for inverted ordering. These model-predicted ranges are well contained within the corresponding NuFIT 6.0 3σ allowed region, $\theta_{12} \in [31.63^\circ, 35.95^\circ]$, for both mass orderings.

6 Results and Discussion: A_4 -Symmetric Double Seesaw

In this section, we present a detailed phenomenological analysis of neutrino masses and mixing predicted within the double seesaw-invoked A_4 flavor symmetry framework. Starting

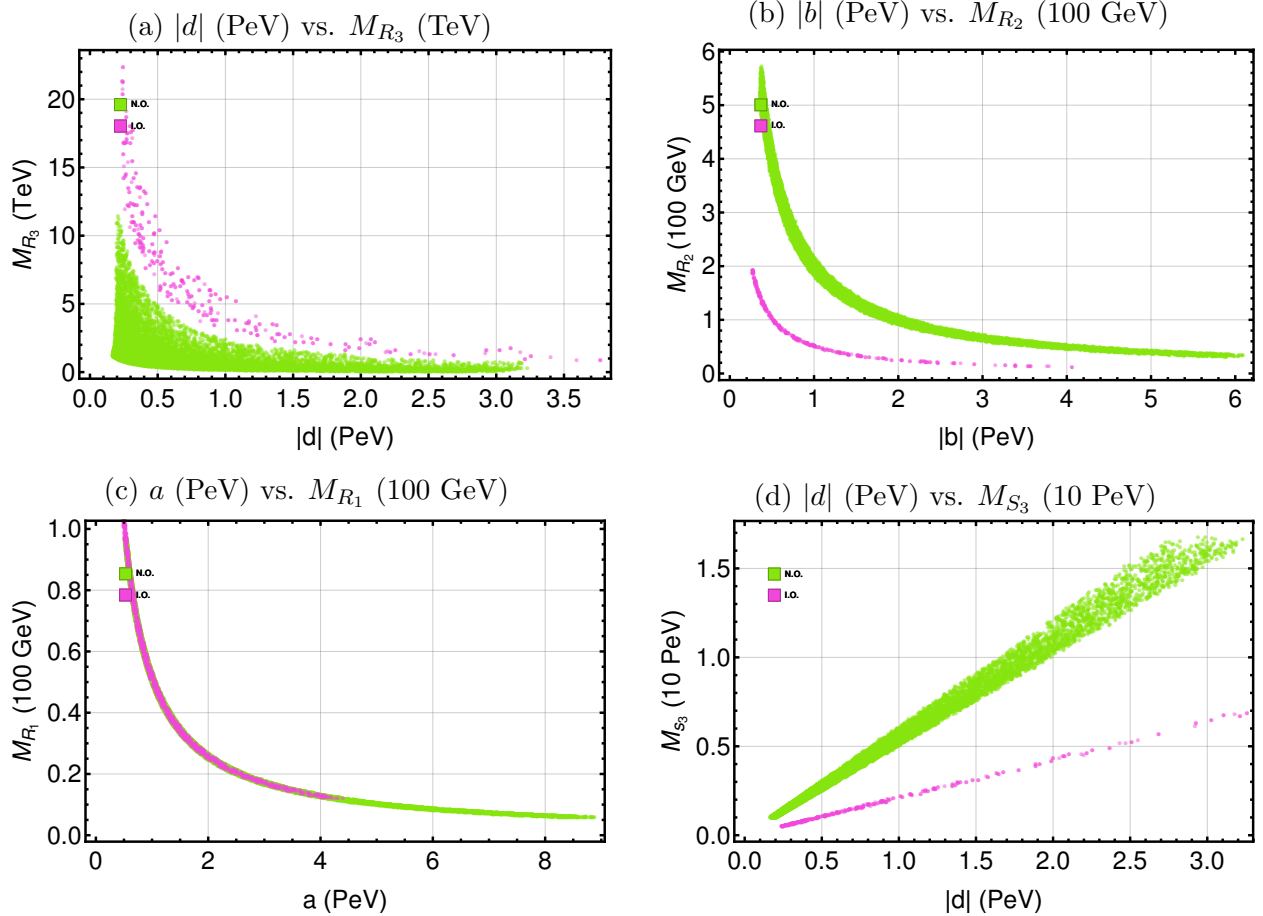


Figure 1: Correlation plots between the high-scale model parameters (a, b, d) and the masses of the right-handed neutrinos ($M_{R_1}, M_{R_2}, M_{R_3}$) and largest mass eigenvalue of the sterile neutrinos M_{S_3} in the double seesaw–invoked A_4 framework. Green (pink) points correspond to normal (inverted) mass ordering.

from the effective light neutrino mass matrix derived in the previous section, we extract the neutrino mass eigenvalues, neutrino mixing angles, and the Dirac CP-violating phase using analytical expressions obtained from the diagonalization procedure. These theoretical predictions are then examined with the most recent global fits of neutrino oscillation data. The free parameters of the model are systematically constrained by imposing the experimentally allowed 3σ ranges of the neutrino mass-squared differences and mixing angles, as reported by the latest NuFIT global analysis. Both normal ordering (NO) and inverted ordering (IO) of neutrino masses are analyzed separately. The combined effects of the underlying A_4 -symmetric mass structures and the double seesaw mechanism lead to characteristic correlations among neutrino observables, which are explored through extensive numerical scans of the parameter space. The resulting predictions for the absolute neutrino mass scale, the Dirac CP phase, and other low-energy observables are critically assessed by comparing the model predictions with current oscillation data.

For a given set of the underlying parameters (a, b, d, k_{RS}, k_D), the eigenvalues of the light

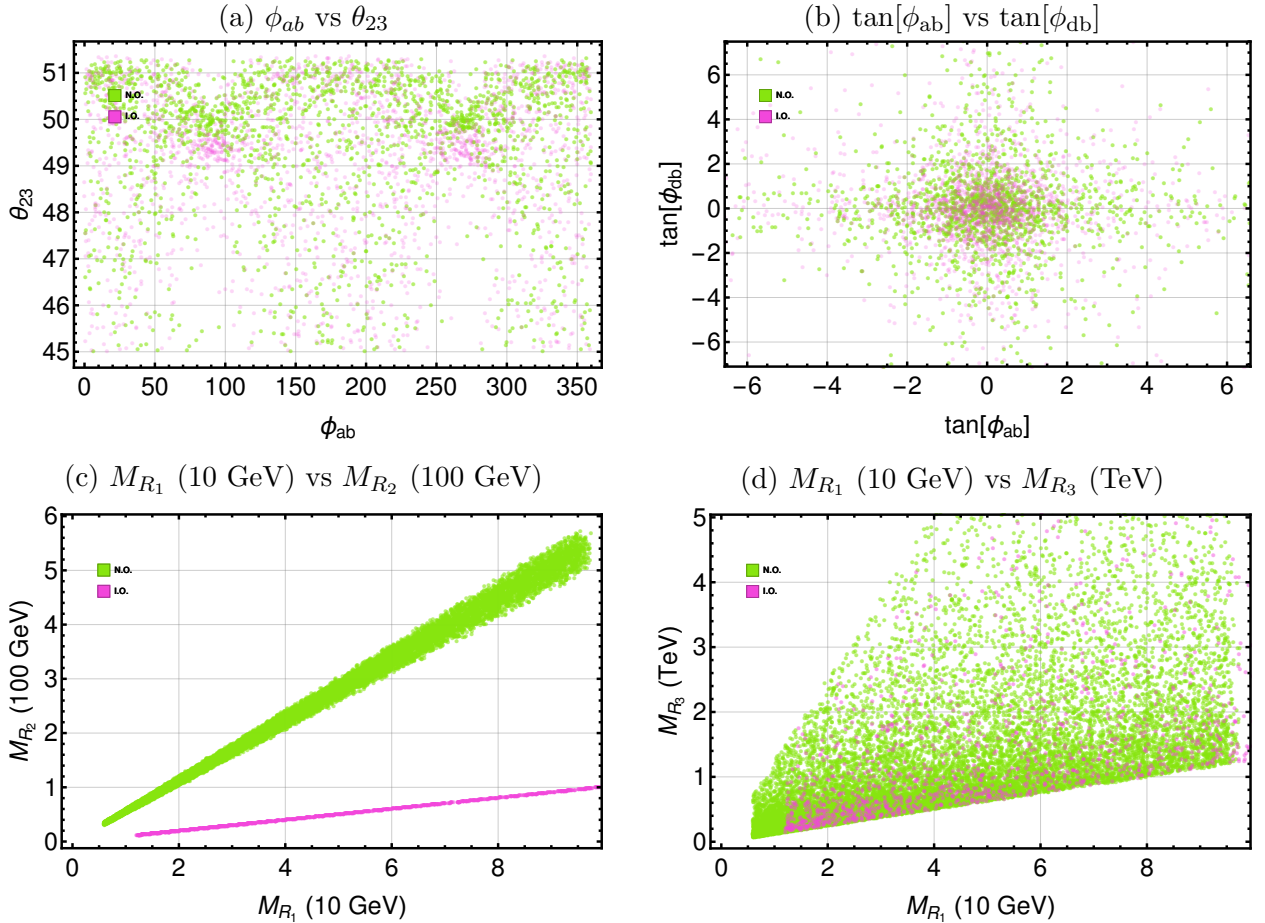


Figure 2: Correlation plots involving right-handed neutrino masses and mixing angle vs. CP phases in the double seesaw-invoked A_4 framework. Green (pink) points correspond to normal (inverted) ordering.

neutrino mass matrix (m_1, m_2, m_3) are computed as presented in Table.2-3 and further, these parameters can be used to evaluate the mass-squared differences. The model predicts:

$$\Delta m_{21}^2 \in (6.92, 8.05) \times 10^{-5} \text{ eV}^2 \quad (6.1)$$

for both mass orderings, while the atmospheric splittings are found to be

$$\begin{aligned} \Delta m_{31}^2 &\in (2.46, 2.61) \times 10^{-3} \text{ eV}^2 \quad (\text{NO}), \\ \Delta m_{32}^2 &\in (-2.58, -2.43) \times 10^{-3} \text{ eV}^2 \quad (\text{IO}). \end{aligned} \quad (6.2)$$

We presented here the correlations between the input model parameters (a, b, d) of the A_4 -symmetric sterile sector and the resulting mass eigenvalues of the right-handed neutrinos and sterile neutrinos. It is clear from the panels (a)–(c) of Fig. 1 that the right-handed neutrino masses $M_{R_i} i = 1, 2, 3$ are not independent but are tightly correlated with the underlying model parameters a, b , and d through the double seesaw relations. In particular, the nearly linear trends observed in $|d| - M_{R_3}$ and $a - M_{R_1}$ reflect the hierarchical structure induced by

the sterile-sector mass matrix M_S . Panel (d) further shows a strong correlation between $|d|$ and the heavy sterile mass M_{S_3} , highlighting the role of the A_4 symmetry in restricting the allowed high-scale parameter space. The substantial overlap between the normal and inverted ordering regions indicates that these correlations are largely insensitive to the light-neutrino mass hierarchy and represent robust predictions of the model. Such structured relationships among high-scale parameters and heavy neutrino masses are particularly relevant for phenomenological studies of lepton-number violation and potential collider signatures of right-handed neutrinos.

In Fig 2, panel-a gives us substantial evidence that atmospheric mixing angle θ_{23} is strongly influenced by the phase ϕ_{ab} . Its panel-b projects the correlation between the phases ϕ_{ab} and ϕ_{db} which indicates a strong phase mixing and dependence on one another along a particular trajectory. Panels (c, d) shows the correlation among the right-handed neutrinos confirming the fact that the mass ratios in the heavy neutrino spectrum can be fixed to produce light neutrino masses in the allowed parameter space. Panel-d shows the direct correlation between the lightest and the heaviest right-handed neutrinos that vividly reflects the hierarchy existing among the heavy RH masses as imposed by the double seesaw mechanism.

Figure 3 illustrates the nontrivial correlations between the internal CP phases (ϕ_{ab}, ϕ_{db}) originating from the A_4 -symmetric sterile sector and the low-energy Dirac CP phase $\psi \simeq \delta_{CP}$, as well as their impact on the atmospheric mixing angle θ_{23} . Panels (a) and (c) demonstrate that ψ is not uniformly distributed but instead exhibits a structured dependence on the underlying phases ϕ_{ab} and ϕ_{db} , reflecting the restricted phase freedom of the model. In panels (b) and (d), a clear correlation between θ_{23} and the CP phases is observed, with the allowed points predominantly populating the higher-octant region $\theta_{23} > 45^\circ$ for both normal and inverted orderings. The near overlap of NO and IO regions indicates that these correlations are largely hierarchy-independent and constitute robust predictions of the double seesaw-invoked A_4 framework. Such characteristic phase-mixing correlations provide a potential avenue for testing the model through future precision measurements of δ_{CP} and θ_{23} .

Overall, the results presented in this subsection demonstrate that the double seesaw-invoked A_4 framework successfully reproduces the observed pattern of neutrino mixing angles while significantly restricting their allowed ranges. This high degree of predictivity provides a strong motivation for studying the detailed correlations among neutrino observables and high-scale parameters, which we address in the next subsection through an analysis of correlation plots.

From Fig 3 (b), ϕ_{db} vs θ_{23} we find that the points are more clustered in the region $45^\circ - 51^\circ$ of θ_{23} indicating that our model strongly favors the higher octant of the atmospheric mixing angle θ_{23} for both normal and inverted orderings ($\theta_{23} > 45^\circ$). In our model we have previously computed that $\psi \approx \delta_{cp}$. Thus the δ_{cp} in our model span within a limited range and it correlates with ϕ_{ab} and ϕ_{db} within the allowed 3σ parameter space as shown in Fig 3. To visualize the dependence of oscillation observables on the underlying model parameters, we present a series of correlation plots and the emergence of discrete, symmetric patterns reflect the highly constrained nature of the A_4 -symmetric double seesaw framework. In particular, Fig. shows a strong clustering of points in the region $\theta_{23} > 45^\circ$, indicating a preference for the higher octant.

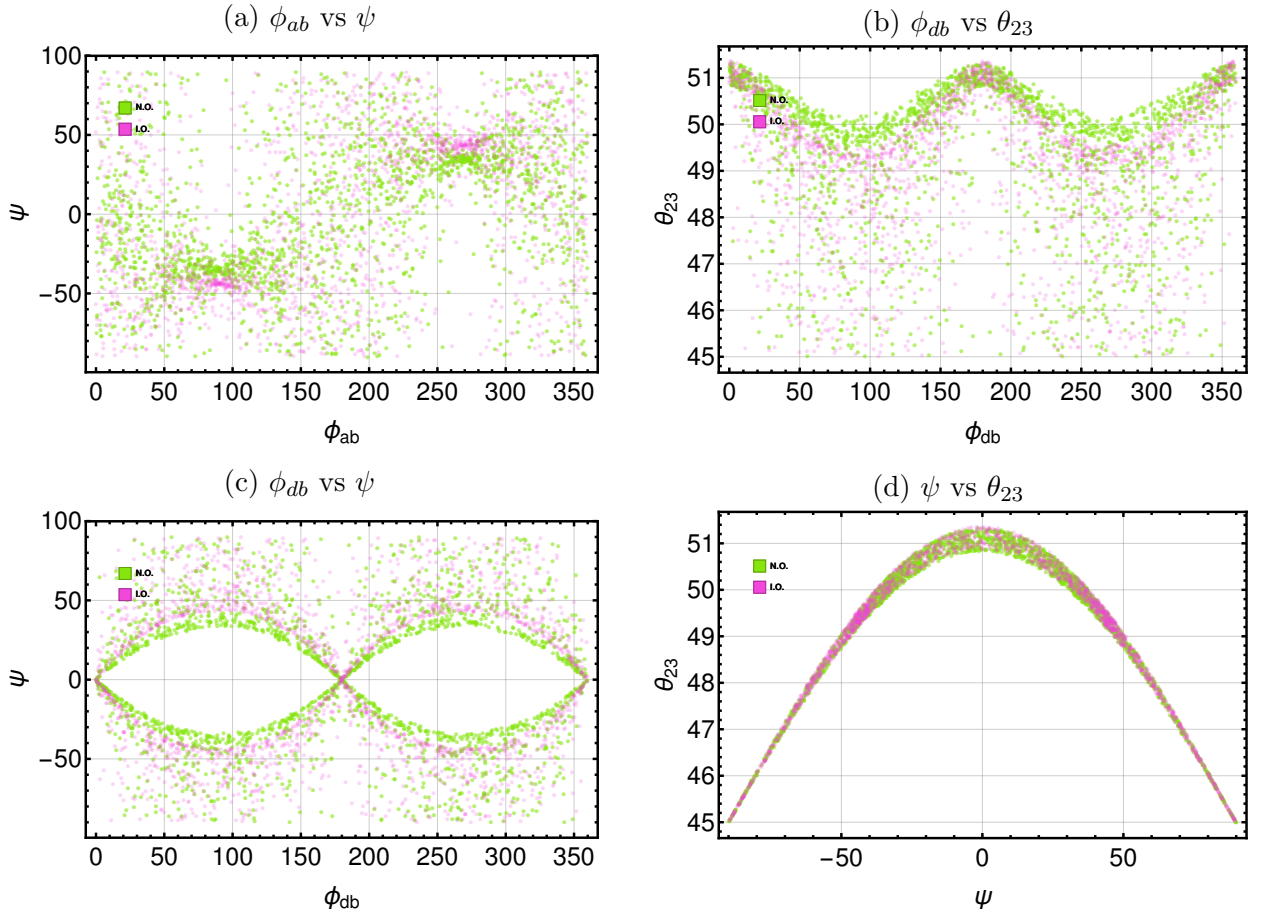


Figure 3: Correlation plots among CP-violating phases and the atmospheric mixing angle in the double seesaw-invoked A_4 framework. Panels show (a) ϕ_{ab} vs ψ , (b) ϕ_{ab} vs θ_{23} , (c) ϕ_{db} vs ψ , and (d) ψ vs θ_{23} . Green (pink) points correspond to normal (inverted) mass ordering.

In Fig 4, panel -(a) indicated that a small change in the sterile mass M_{S_2} would increase the parameter b which is much needed to obtain light neutrino masses of the correct order. Panel-(b) shows that the parameter a is tightly correlated with the sterile masses. This co-dependency sets the neutrino mass scale that is consistent with the double seesaw mechanism. Here the panels (c, d) simply shows the interrelation between the masses in the sterile sector to form a viable mass structure.

6.1 Impact on Solar Neutrino Parameters from JUNO first data and other experimental solar measurements

The solar neutrino oscillation parameters provide a stringent test of flavor models, particularly those predicting correlated structures among mixing angles and mass splittings. We intend here to examine whether or not the expected values of the neutrino mixing angles and mass-square differences in our double seesaw-invoked A_4 framework are within the experimental limit set by the ongoing or future planned experiments.

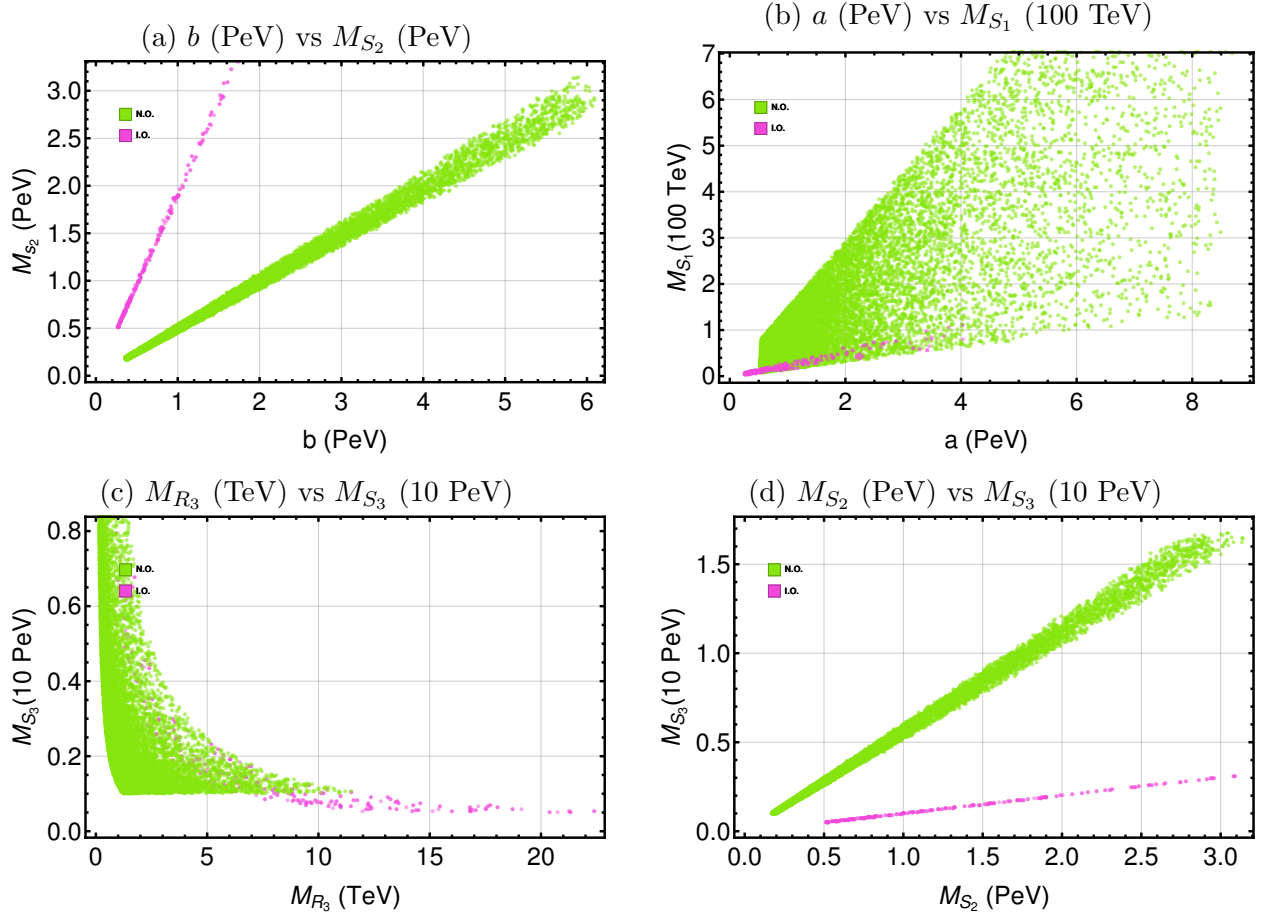


Figure 4: Correlation plots among sterile-sector masses and model parameters in the double seesaw-invoked A_4 framework. Green (pink) points denote normal (inverted) ordering.

Recently, the Jiangmen Underground Neutrino Observatory (JUNO [40]) collaboration reported the first simultaneous high-precision determination of the solar mixing angle θ_{12} and the mass-squared difference Δm_{21}^2 assuming normal mass ordering (NO). The reported values are

$$\Delta m_{21}^2 = m_2^2 - m_1^2 = (7.50 \pm 0.12) \times 10^{-5} \text{ eV}^2, \quad \sin^2 \theta_{12} = 0.3092 \pm 0.0087, \quad (6.3)$$

corresponding to sub-percent and percent-level precision, respectively. This marks a substantial improvement over earlier reactor measurements, with JUNO reducing the uncertainty in Δm_{21}^2 to approximately 1.55%. For comparison, the KamLAND [73] experiment reported the solar mass-squared difference as $\Delta m_{21}^2 = (7.53^{+0.18}_{-0.18}) \times 10^{-5} \text{ eV}^2$ corresponding to an uncertainty of approximately 2.81% while KamLAND data taken in 2013, from a combined three-flavored analysis of solar neutrino oscillation, reported the value of the solar mixing angle as $\tan^2 \theta_{12} = 0.436^{+0.029}_{-0.025}$ and $\Delta m_{21}^2 = 7.53^{+0.18}_{-0.18} \times 10^{-5} \text{ eV}^2$ [73]. More recently, the phase-IV analysis of Super-Kamiokande (SK-IV) [74], based on solar neutrino data, reported

$$\sin^2 \theta_{12} = 0.306 \pm 0.013, \quad \Delta m_{21}^2 = (6.10^{+0.95}_{-0.81}) \times 10^{-5} \text{ eV}^2, \quad (6.4)$$

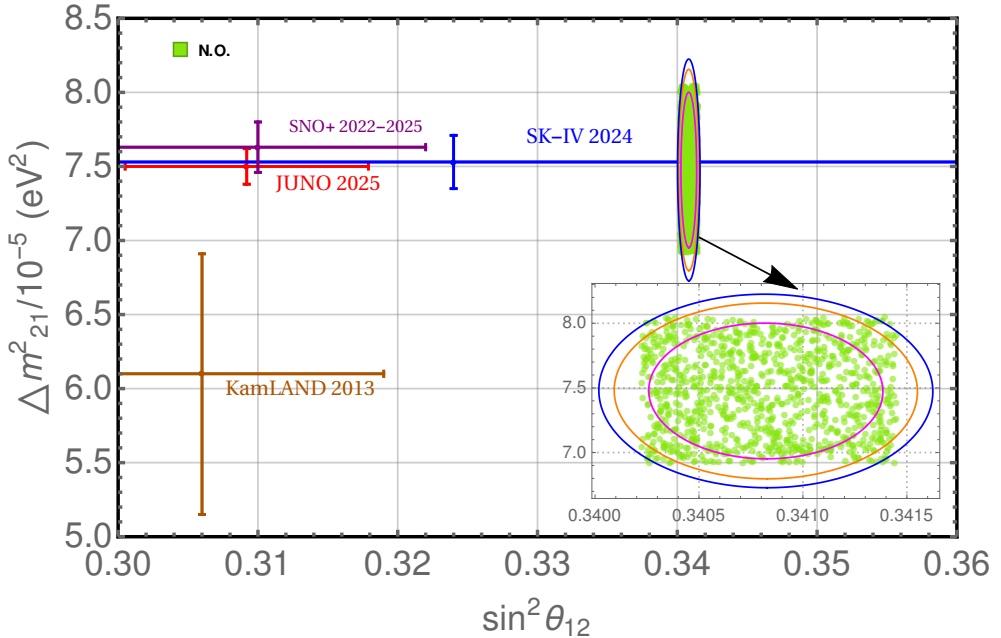


Figure 5: Correlation plot between measured value of $\sin^2 \theta_{12}$ vs $\Delta m_{21}^2/10^{-5}$ eV 2 . The blue, orange and red contours in the magnified plot corresponds to 3σ , 2σ , 1σ allowed parameter space of $\sin^2 \theta_{12}$ vs $\Delta m_{21}^2/10^{-5}$ eV 2 while the green points correspond to the double seesaw-invoked A_4 symmetry model prediction.

Our model derived limits $\Delta m_{21}^2 \in [6.92, 8.05] \times 10^{-5}$ eV 2 align well with the experimental limits of JUNO (2025) KamLAND (2013), SK-IV limits (2024) and our model based limit $\sin^2 \theta_{12} \in 0.3407 \pm 0.006$ falls within the limits ventured by the experiments KamLAND (2013), and NuFIT 6.0 neutrino oscillation analysis. The correlation between the solar mixing parameter $\sin^2 \theta_{12}$ and the mass-squared difference Δm_{21}^2 obtained from a scan over the viable parameter space of the present double seesaw-invoked A_4 framework is shown in Fig.5 displayed in green dotted points. The colored contours in the magnified inset correspond to the 1σ (red), 2σ (orange), and 3σ (blue) confidence regions, while the green points denote model solutions consistent with all theoretical and phenomenological constraints of the present framework. The superimposed experimental bands represent the recent precision determination from the JUNO 2025 projection, along with earlier measurements from KamLAND-2013 [73] and Super-Kamiokande-IV (2024) [74]. The allowed region clearly favors normal mass ordering (N.O.), which emerges naturally in our framework as a consequence of the A_4 -symmetric structure of the light neutrino mass matrix and the hierarchical suppression inherent to the double seesaw mechanism. A pronounced correlation between $\sin^2 \theta_{12}$ and Δm_{21}^2 is observed, reflecting the reduced parameter freedom imposed by the flavor symmetry. Importantly, the JUNO-preferred region of Δm_{21}^2 is well contained within the 1σ - 2σ contours of our model, indicating excellent compatibility without fine-tuning. Given JUNO's anticipated sub-percent sensitivity to both Δm_{21}^2 and $\sin^2 \theta_{12}$, future data will decisively test this correlation, rendering the present double seesaw realization with A_4 symmetry highly predictive and potentially falsifiable in the solar neutrino sector.

In addition, the SNO+ collaboration reported $\Delta m_{21}^2 = (7.63 \pm 0.17) \times 10^{-5} \text{ eV}^2$ and $\sin^2 \theta_{12} = 0.310 \pm 0.012$ from reactor antineutrino data collected between May 2022 and July 2025 [75]. It is also to be noted that Solar+KamLAND records $\Delta m_{21}^2 / 10^{-5} \approx 7.50_{-0.18}^{+0.19}$, $\sin^2 \theta_{12} = 0.307 \pm 0.012$ [74] and Solar global records $\Delta m_{21}^2 / 10^{-5} \approx 6.10_{-0.81}^{+0.95}$, $\sin^2 \theta_{12} = 0.303 \pm 0.013$ [74]. These data were recorded from October 2008 to May 2018 (2970 days) from the fourth phase of Super Kamiokande (SK IV) for events of solar neutrinos energies of 3.49 - 19.49 meV. Most of these measurements are in excellent agreement with the model-predicted ranges, thereby reinforcing the robustness of the double seesaw-invoked A_4 framework.

6.2 Impact on Atmospheric Neutrino Parameters from atmospheric data from Deep Core Ice-Cube and LBL experiments

Atmospheric neutrino measurements further constrain the atmospheric neutrino parameter space obtained from our model. The Deep Core Ice-Cube Neutrino Observatory analyzed neutrinos with energies above 5 GeV. Based on this 3387 days of data (2012-2021), Deep-Core Ice-Cube reports $\Delta m_{32}^2 = 2.40_{-0.04}^{+0.05} \times 10^{-3} \text{ eV}^2$ and $\sin^2 \theta_{23} = 0.54_{-0.03}^{+0.04}$ [76]. Similarly, the Super Kamiokande analyzed the data set taken from phase I to phase V (SK I-V) (from April 1996 to July 2020) and based on it reported that $\Delta m_{32}^2 = 2.40_{-0.09}^{+0.07} \times 10^{-3} \text{ eV}^2$, $\sin^2 \theta_{23} = 0.45_{-0.05}^{+0.06}$ and $\delta_{CP} = -1.75_{-1.25}^{+0.76}$ [77]. Our model predicted range of δ_{CP} is $[-89.99^\circ, 89.99^\circ]$ for both ordering, $\Delta m_{32}^2 \sim [2.455 \pm 0.065 \times 10^{-3} \text{ eV}^2]$ for normal ordering and $\sin^2 \theta_{23} = 0.5545 \pm 0.0545$ (0.555 ± 0.055) for NO (IO), which is consistent with these experimental observations.

Long-baseline accelerator experiments provide complementary constraints. The NO ν A recently recorded high precision measurements as: $\Delta m_{32}^2 = 2.431_{-0.034}^{+0.036} (-2.479_{-0.036}^{+0.036}) \times 10^{-3} \text{ eV}^2$ for NO (IO). In both ordering $\sin^2 \theta_{23} = 0.55_{-0.02}^{+0.06}$ is the preferred parameter range. However it is interesting to note that this data set of three flavor neutrino oscillation mildly prefers normal ordering with 2.4 times more probability than inverted ordering [78]. Joint analyses from T2K and NO ν A constrain δ_{CP} within $[-1.38\pi, 0.30\pi]$ (NO) and $[-0.92\pi, -0.04\pi]$ for IO [79], without a strong preference for mass ordering. The KM3NeT/ORCA atmospheric neutrino analysis disfavors inverted ordering and reports $\sin^2 \theta_{23} = 0.51_{-0.05}^{+0.04}$ and $\Delta m_{31}^2 = (2.18_{-0.35}^{+0.25}) \times 10^{-3} \text{ eV}^2$ (NO) [80], again compatible with our predictions.

6.3 Synergy between mixing angles and phases

In this subsection, we analyze the correlations among the CP-violating phases and the atmospheric mixing angle that emerge from the double seesaw-invoked A_4 framework. These correlations arise from the constrained phase structure of the sterile-sector Majorana mass matrix and its propagation to low-energy observables through the double seesaw mechanism. The resulting patterns provide valuable insight into the predictability of the model and its sensitivity to future precision measurements.

Using the analytical expressions derived in Eqs. (4.7) and (4.9), we predict the allowed ranges of the solar and atmospheric mixing angles θ_{12} and θ_{23} within the double seesaw-

invoked A_4 framework. To confront these predictions with experimental data, we take the 3σ range of θ_{13} from the NuFIT 6.0 global analysis [72] as an external input. Owing to the constrained structure of the light neutrino mass matrix dictated by the A_4 symmetry and the double seesaw scaling, the model yields a remarkably narrow range for the solar mixing angle,

$$\begin{aligned}\theta_{12} &\in [35.68^\circ, 35.75^\circ] \quad (\text{NO}), \\ \theta_{12} &\in [35.68^\circ, 35.76^\circ] \quad (\text{IO}),\end{aligned}\quad (6.5)$$

which lies well within the corresponding NuFIT 6.0 3σ allowed interval, $\theta_{12} \in [31.63^\circ, 35.95^\circ]$, for both mass orderings. This strong restriction is a direct manifestation of the reduced parameter freedom inherent to the A_4 -symmetric realization of the double seesaw mechanism.

Figure 6 presents a comparison of the model-predicted values of $\sin^2 \theta_{12}$ with the allowed regions obtained from various solar and reactor neutrino experiments. The figure clearly shows that the model predictions lie well inside the experimentally allowed bands, including the recent high-precision determination of the solar mixing angle, thereby demonstrating the consistency of the framework with current data. The solar experimental data that we have considered here are from NuFIT6.0 [81], SNO [82], KamLAND [83], JUNO [40], SNO+ [75], Solar+KamLAND [74], Solar global [74]. All these experimental limits can be found in [84].

The atmospheric mixing angle θ_{23} exhibits a similarly constrained behavior. In Fig. 7,

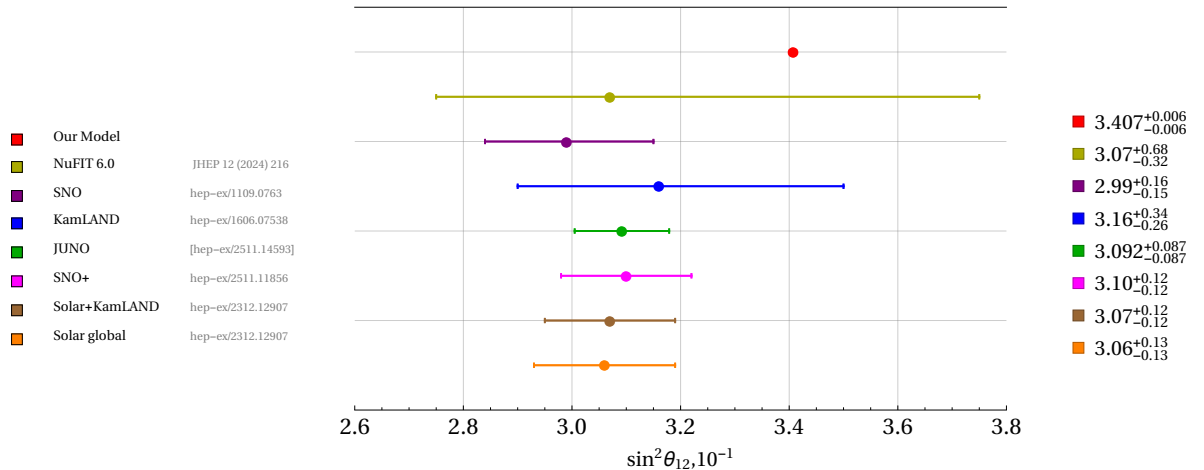


Figure 6: Comparison of the model-predicted solar mixing angle $\sin^2 \theta_{12}$ with the experimentally allowed regions from global fits and reactor/solar neutrino experiments. The narrow band corresponds to the predictions of the double seesaw-invoked A_4 framework. The experimental limits presented here are taken from Refs. [40, 72, 74, 75, 82–84].

we show the comparison between the model predictions for $\sin^2 \theta_{23}$ and the experimental limits for normal ordering. The majority of the allowed points cluster in the higher octant, $\theta_{23} > 45^\circ$, reflecting a characteristic prediction of the model arising from the interplay between the A_4 symmetry and the double seesaw hierarchy.

Figure 8 shows the corresponding comparison for inverted ordering. As in the normal ordering case, the predicted values of θ_{23} remain consistent with the current experimental

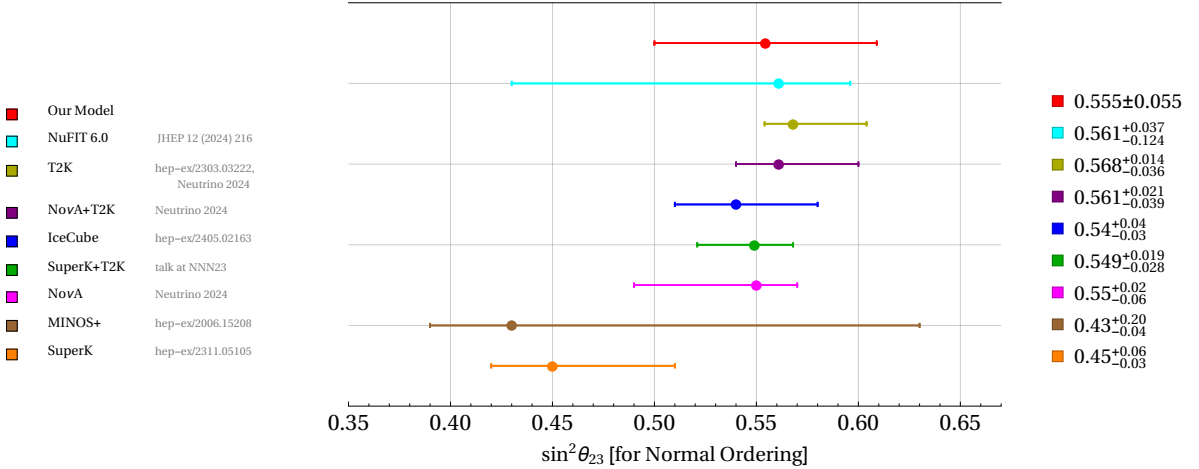


Figure 7: Comparison of the atmospheric mixing angle $\sin^2 \theta_{23}$ predicted by the model with experimental limits for normal mass ordering. The shaded regions indicate the experimentally allowed ranges, while the model points predominantly favor the higher octant. The experimental limits presented here are taken from Refs. [72, 76, 77, 85–88].

bounds and continue to exhibit a preference for the higher octant. The similarity between the NO and IO predictions highlights the robustness of the model against the choice of mass hierarchy, while still maintaining strong correlations among the mixing parameters.

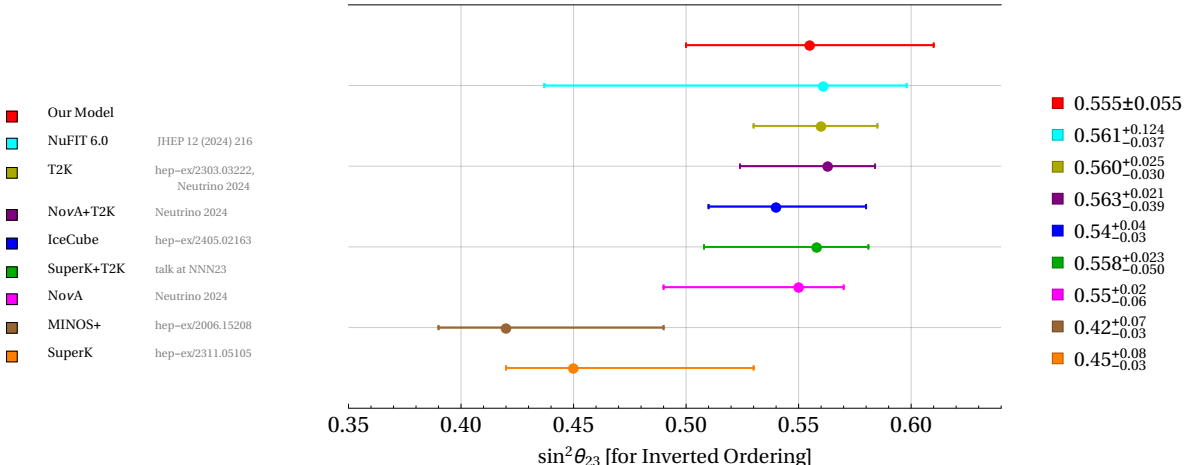


Figure 8: Comparison of the atmospheric mixing angle $\sin^2 \theta_{23}$ predicted by the model with experimental limits for inverted mass ordering. The model remains compatible with the global-fit ranges and continues to favor θ_{23} in the higher octant.

The atmospheric mixing angle is predicted to lie within

$$\begin{aligned} \theta_{23} &\in [45.00^\circ, 51.33^\circ] \quad (\text{NO}), \\ \theta_{23} &\in [45.00^\circ, 51.36^\circ] \quad (\text{IO}), \end{aligned} \quad (6.6)$$

at the 3σ level. Most of the model-generated points overlap with the NuFIT 6.0 allowed regions, $\theta_{23} \in [41.0^\circ, 50.5^\circ]$ (NO) and $[41.4^\circ, 50.6^\circ]$ (IO), indicating a mild preference for

the higher octant of θ_{23} inherent to the model.

6.4 Neutrinoless Double Beta Decay Implications from JUNO data

Neutrinoless double beta decay ($0\nu\beta\beta$) provides a unique probe of the Majorana nature of neutrinos and is directly sensitive to the effective Majorana mass parameter m_{ee} , which depends on the neutrino masses, Majorana phases, and the leptonic mixing angles, in particular θ_{12} and θ_{13} . Consequently, any improvement in the precision of oscillation parameters has a direct and quantitatively significant impact on the allowed range of m_{ee} for both normal (NO) and inverted (IO) mass orderings. The implications of the recent JUNO precision measurements extend beyond oscillation phenomenology and play a crucial role in constraining the effective Majorana mass parameter m_{ee} relevant for neutrinoless double beta ($0\nu\beta\beta$) decay. This naturally leads us to the study of neutrinoless double beta decay ($0\nu\beta\beta$),

$${}^A_Z N \rightarrow {}^A_{Z+2} N + 2e^-, \quad (6.7)$$

a lepton-number-violating process in which no neutrinos are emitted and only two electrons appear in the final state. Such a decay can occur if neutrinos are Majorana particles, and its amplitude is governed by the effective Majorana mass parameter m_{ee} , defined as

$$|m_{ee}| = \left| |U_{e1}^2| m_1 + |U_{e2}^2| m_2 e^{i\alpha} + |U_{e3}^2| m_3 e^{i\beta} \right| \quad (6.8a)$$

$$= |c_s^2 c_r^2 m_1 + s_s^2 c_r^2 m_2 e^{i\alpha} + s_r^2 m_3 e^{i\beta}|. \quad (6.8b)$$

Here, m_i are denoting the mass eigenvalues for light neutrinos while the Majorana phases are denoted as α, β . Also, U_{ei} represents the elements of PMNS mixing matrix and used the notation for mixing angles as $(c_\alpha, s_\alpha) \equiv (\cos \theta_\alpha, \sin \theta_\alpha)$ where $\theta_a \equiv \theta_{23}$ is the atmospheric mixing angle, $\theta_r \equiv \theta_{13}$ is the reactor mixing angle and $\theta_s \equiv \theta_{12}$ as the solar mixing angle.

Figure 9 illustrates the resulting 3σ allowed bands in the m_{ee} – m_{lightest} plane obtained by varying the neutrino oscillation parameters from the global fit data from NuFIT-6.0 [72], overlaid with the updated JUNO constraints and the predictions of our model. The light-blue and light-red shaded regions in Fig. 9 correspond to the experimentally allowed ranges for normal and inverted orderings while the colored points represent the predictions arising from the double seesaw–invoked A_4 flavor framework. The overlapping region of the NO and IO represents for the quasi-degenerate (QD) spectrum which has already been disfavored from the KATRIN and PLANCK data. The translated limit on lightest neutrino mass has been derived from the experimental limit on sum of light neutrino masses and at present, the bound on the sum of neutrino masses from PLANCK is $\sum m_\nu < 0.12$ eV at 95% C.L. [92] while KATRIN [93] experiment provides the direct limit on absolute active neutrino mass ($m_\nu < 0.45$ eV at 90% CL).

Because of the restricted structure of the light neutrino mass matrix enforced by the A_4 symmetry and the hierarchical suppression intrinsic to the double seesaw mechanism, the model predicts a narrow and correlated range of $m_{ee} \in 0.057 - 6.88$ meV (14.87 – 49.31 meV)

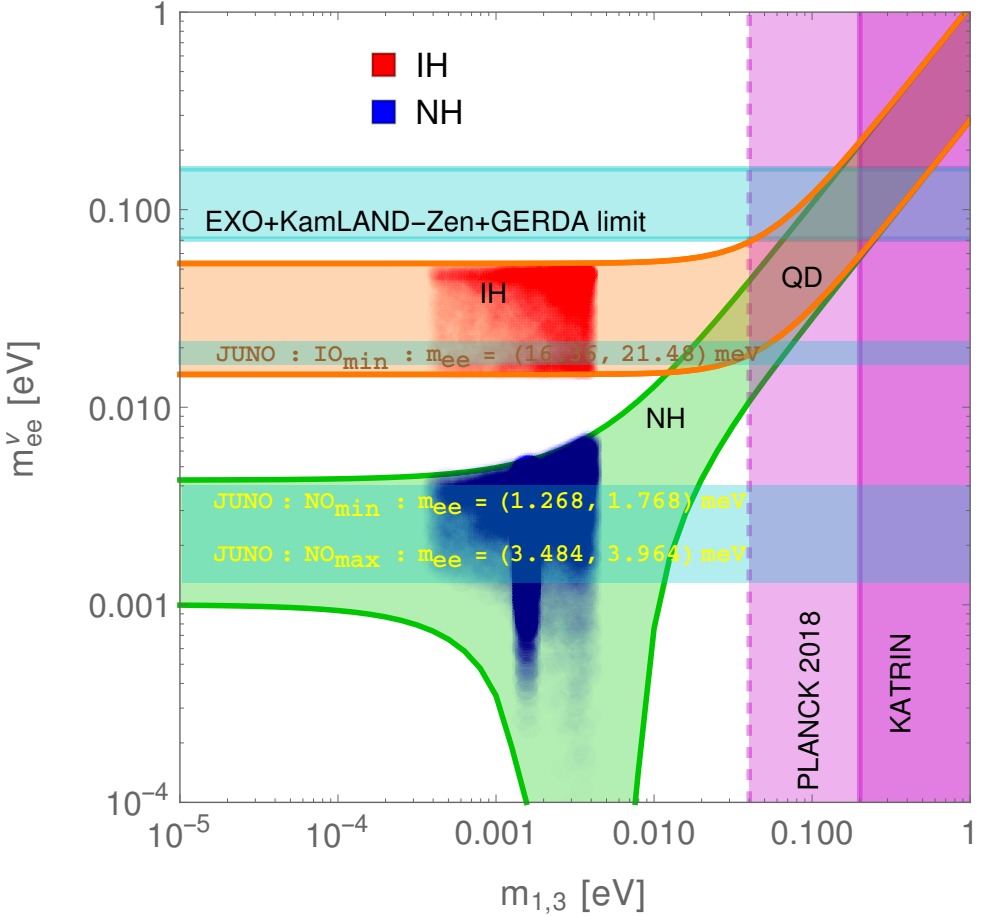


Figure 9: Effective Majorana mass parameter $m_{ee}^{\nu} \equiv m_{ee}$ with the variation of lightest neutrino mass m_1 (or m_3) for normal ordering (NO) and inverted ordering (IO). The cyan horizontal band represents the experimental limits by KamLAND-Zen (28 – 122 meV) [89, 90] and GERDA (79 – 118 meV) [91].

for NO (IO), fully consistent with the JUNO-updated 3σ intervals. The recent first data release from the JUNO experiment has led to a substantial reduction in the uncertainties of the solar mixing angle θ_{12} and the mass-squared difference Δm_{21}^2 . This improved precision propagates into tighter constraints on m_{ee} , as explicitly demonstrated in Ref. [94]. In particular, the relative uncertainties in the determination of m_{ee} have been reduced to 22.0% for $\langle m_{ee} \rangle_{\text{min}}^{\text{IO}}$, 22.5% for $\langle m_{ee} \rangle_{\text{min}}^{\text{NO}}$, and 23.1% for $\langle m_{ee} \rangle_{\text{max}}^{\text{NO}}$. As a result, the updated 3σ intervals inferred using JUNO first data are

$$\begin{aligned} \langle m_{ee} \rangle_{\text{min}}^{\text{IO}} &= (16.36, 21.48) \text{ meV}, \\ \langle m_{ee} \rangle_{\text{min}}^{\text{NO}} &= (1.268, 1.768) \text{ meV}, \\ \langle m_{ee} \rangle_{\text{max}}^{\text{NO}} &= (3.484, 3.964) \text{ meV}. \end{aligned} \quad (6.9)$$

The present experimental limits on the effective Majorana mass are provided by GERDA (79 – 118 meV) [91], LEGEND 200 (75 – 200 meV) [95] for ${}^{76}\text{Ge}$ isotope, EXO [96], KamLAND-

Zen (28 – 122 meV [90]) for ^{136}Xe isotope, and **CUORE** (70 – 240 meV [97]) for ^{130}Te isotope. Of particular importance is the fact that the upper range of $\langle m_{ee} \rangle_{\text{max}}$ for normal ordering falls within the projected sensitivity of forthcoming next-generation $0\nu\beta\beta$ experiments. Experiments such as **nEXO** (^{136}Xe) [98, 99] and **LEGEND-1000** (^{76}Ge) [100] aim to reach sensitivities of $m_{ee} \simeq 6 - 27$ meV and $m_{ee} \simeq 9 - 21$ meV, respectively, while **CUPID** targets a sensitivity of $m_{ee} \simeq 12 - 34$ meV [101, 102].

The model predicts narrow allowed regions for both mass orderings, consistent with current experimental limits from the **GERDA**, **KamLAND-Zen** and **LEGEND 200** experiments. Importantly, the predicted m_{ee} ranges fall within the reach of next-generation experiments like **nEXO**, **LEGEND-1000**, offering a realistic opportunity to test the model. Finally, the presence of Majorana neutrino masses and CP-violating phases in the double seesaw-invoked A_4 framework naturally provides the ingredients required for leptogenesis, thereby linking neutrino properties with the origin of the baryon asymmetry of the Universe. The synergy between **JUNO**’s precision oscillation measurements and these upcoming $0\nu\beta\beta$ searches therefore renders the present double seesaw-invoked A_4 framework highly predictive and experimentally testable, with the potential to either confirm or decisively constrain the model in the near future.

6.5 Correlation between Dirac CP Phase and Jarlskog Invariant

Jarlskog invariant measures the correlation between the Dirac CP-violating phase δ and the leptonic Jarlskog invariant J_{CP} [103–106]. We now intend to estimate the value of J_{CP} with the variation of the Dirac CP-violating phase δ within the framework of an A_4 flavor symmetric double seesaw mechanism, for both normal ordering (NO) and inverted ordering (IO) of neutrino masses. As seen from Fig. 10, the Jarlskog invariant exhibits a smooth and monotonic dependence on the Dirac CP phase and changes sign as δ crosses zero. The horizontal axis represents the Dirac CP phase δ (in degrees), while the vertical axis denotes the Jarlskog invariant J_{CP} , which provides a rephasing-invariant measure of CP violation in the lepton sector. This behavior follows directly from the general relation

$$J_{\text{CP}} = \frac{1}{8} \sin 2\theta_{12} \sin 2\theta_{23} \sin 2\theta_{13} \cos \theta_{13} \sin \delta, \quad (6.10)$$

which holds for the standard parametrization of the PMNS matrix. Consequently, CP conservation is recovered for $\delta = 0^\circ$ and $\delta = \pm 180^\circ$, while maximal CP violation occurs near $\delta \simeq \pm 90^\circ$. The predicted magnitude of the Jarlskog invariant in the present A_4 double seesaw framework lies in the range

$$|J_{\text{CP}}| \simeq (3-4) \times 10^{-2}, \quad (6.11)$$

which is consistent with current global-fit results of neutrino oscillation data. Notably, the predictions corresponding to normal and inverted mass orderings largely overlap, indicating that the correlation between δ and J_{CP} is only weakly sensitive to the neutrino mass hierarchy. This feature originates from the dominant role played by the A_4 -symmetric flavor structure of the mass matrices. Fig. 10 demonstrates that the A_4 flavor symmetric double seesaw model

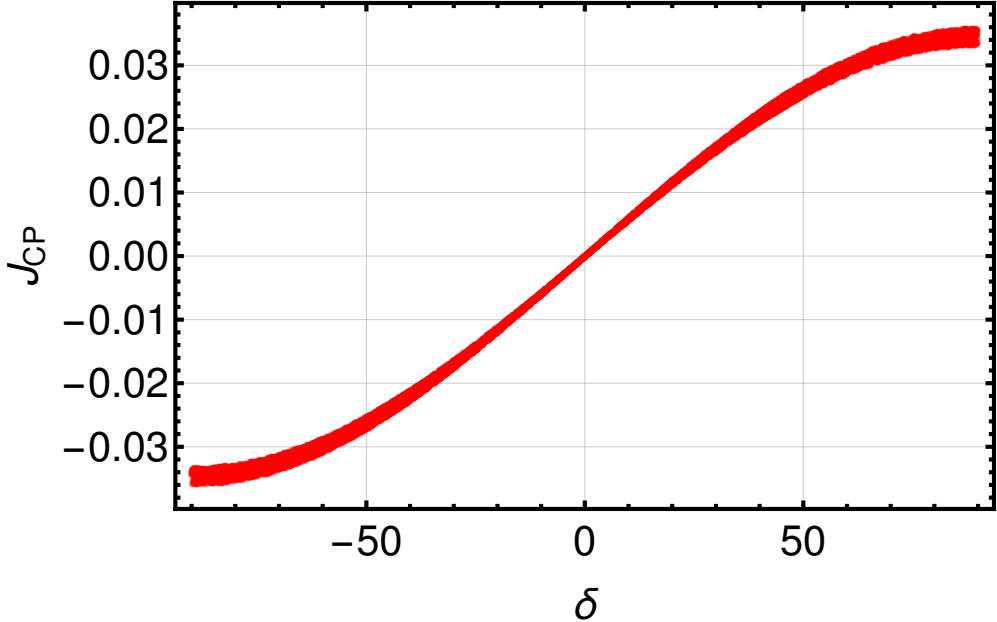


Figure 10: Correlation plot between Dirac CP phase δ and the Jarlskog invariant J_{CP} for both IO and IO case.

naturally accommodates sizable leptonic CP violation and predicts a well-defined correlation between the Dirac CP phase and the Jarlskog invariant. These predictions can be tested in current and upcoming long-baseline neutrino oscillation experiments such as T2K, NO ν A, DUNE, and Hyper-Kamiokande.

The recent high-precision results from the JUNO experiment provide an important complementary test of the present framework by significantly improving the determination of the solar mixing angle θ_{12} and the mass-squared difference Δm_{21}^2 , which directly enter the Jarlskog invariant [107, 108]. Using the JUNO-constrained parameter space, we find that the predicted range $|J_{CP}| \simeq (3\text{--}4) \times 10^{-2}$ remains unchanged for both normal and inverted mass orderings. This demonstrates that the δ - J_{CP} correlation predicted by the A_4 flavor-symmetric double seesaw model is robust against the latest precision oscillation data. The synergy between JUNO and forthcoming long-baseline experiments will therefore provide a decisive test of leptonic CP violation in this framework.

7 Conclusion

In this work, we have carried out a comprehensive and systematic study of the double seesaw mechanism embedded within a flavor-symmetric framework governed by the discrete group A_4 . By extending the Standard Model with both right-handed neutrinos and additional gauge-singlet sterile neutrinos, we demonstrated that the interplay between the double seesaw structure and A_4 flavon alignments leads to a highly constrained and phenomenologically predictive neutrino sector. A central outcome of our analysis is that simple and well-motivated A_4 charge assignments for the lepton doublets, right-handed neutrinos, and

sterile fermions naturally yield tightly correlated textures for the Dirac mass matrix M_D , the $N_R - S_L$ mixing matrix M_{RS} , and the sterile Majorana mass matrix M_S . Owing to the characteristic A_4 vacuum alignment, the leading-order prediction for the light neutrino mass matrix exhibits a tri-bimaximal (TBM) mixing structure. Importantly, we showed that a single rotation in the (1–3) sector—induced either by higher-order corrections or by specific A_4 -driven phase factors—is sufficient to generate the experimentally observed reactor mixing angle θ_{13} while preserving the approximate TBM predictions for the solar and atmospheric mixing angles. Thus, the model provides a structurally simple yet realistic framework in which the deviation from TBM originates from a clear symmetry source.

We also derived analytic expressions for the heavy right handed neutrino eigenvalues and the resulting light neutrino masses, enabling us to clearly identify how each sector of the double seesaw contributes to the overall neutrino mass hierarchy. The analytic treatment highlights the role of the A_4 structure in suppressing or enhancing particular mass eigenvalues, thereby offering a transparent understanding of why the model favors a normal mass ordering and how the sterile-sector mass scales are distributed. Further, we incorporated the recent results from JUNO experiment in our numerical analysis which significantly improved the precision of the solar mixing angle, $\sin^2 \theta_{12} \simeq 0.31$, along with the latest global constraints on $\sin^2 \theta_{13}$. We demonstrated that these updated values impose strong restrictions on the model’s parameter space. The improved precision on θ_{12} directly constrains the magnitude of the (1–3) rotational correction required to depart from exact tribimaximal mixing, while the measured value of θ_{13} further restricts the allowed parameter space, including the rotation angle, CP phases, and coupling ratios of the model. Consequently, a considerable portion of the previously allowed parameter space is now excluded, pointing towards a narrower and more predictive region in which the model remains experimentally viable. The constrained structure of the light neutrino mass matrix induces a nontrivial correlation between $\sin^2 \theta_{12}$ and Δm_{21}^2 , leading to a clear preference for normal ordering. Notably, the JUNO best-fit region lies well within the 1σ – 2σ allowed contours of the model, while older measurements span broader regions of the parameter space. Given JUNO’s anticipated sub-percent precision in the solar sector, future data will provide a decisive test of this predicted correlation, thereby rendering the present framework highly predictive and potentially falsifiable.

The predicted values of LNV Majorana mass parameter for neutrinoless double beta decay process are in excellent agreement with the predictions of our double seesaw framework with A_4 flavor symmetry, which yields a restricted and correlated m_{ee} spectrum as a direct consequence of the underlying neutrino mass texture. In particular, the upper range of $\langle m_{ee} \rangle_{\text{max}}$ for normal ordering lies within the projected sensitivity of next-generation $0\nu\beta\beta$ experiments such as nEXO (^{136}Xe) [98, 99] and LEGEND-1000 (^{76}Ge) [100], with expected sensitivities of $m_{ee} \sim (6\text{--}27)$ meV and $(9\text{--}21)$ meV, respectively. Furthermore, the CUPID experiment aims to reach a sensitivity of $m_{ee} \sim (12\text{--}34)$ meV [101, 102]. Therefore, the synergy between JUNO precision oscillation data and upcoming $0\nu\beta\beta$ searches renders the present double seesaw scenario highly predictive and experimentally testable in the near future.

Overall, our investigation shows that the combination of the double seesaw mechanism and A_4 flavor symmetry forms a coherent and robust theoretical framework capable of re-

producing all key features of the observed neutrino oscillation data. The framework not only elucidates the origin of light neutrino masses in a symmetry-driven fashion but also yields experimentally testable predictions, particularly regarding mixing-angle correlations and the hierarchy of sterile-sector masses. With future data from JUNO, DUNE, Hyper-K, and precision cosmology, the parameter space outlined in this work will be tested further, providing a clear pathway to experimentally confirm or refute the viability of this class of double-seesaw, A_4 -motivated models.

Acknowledgement

SP acknowledges the financial support under MTR/2023/000687 funded by SERB, Govt. of India. Two of the authors (CD and SKN) gratefully acknowledge the Institute of Physics (IOP), Bhubaneswar for valuable discussions and support during the preparation of the manuscript.

MRD would like to thank Maxim O. Gonchar (Dubna, JINR and Irkutsk State U.) for giving permission to use the valuable information in his GitLab repository on the recent neutrino experimental findings.

A Predictive Structures of the Double Seesaw Mechanism with A_4 Symmetry

In this appendix, we present the detailed Lagrangian structure and mass matrices of the double seesaw mechanism (DSM) realized within an A_4 flavor symmetry. These results underpin the analytic derivations of neutrino masses, mixing angles, and CP-violating phases discussed in the main text.

Charged-Lepton Sector: The Yukawa interaction responsible for charged-lepton masses is given by

$$\mathcal{L}_\ell = y_\ell^{ee} \bar{L}_{eL} H e_R + y_\ell^{\mu\mu} \bar{L}_{\mu L} H \mu_R + y_\ell^{\tau\tau} \bar{L}_{\tau L} H \tau_R + \text{h.c.}, \quad (\text{A.1})$$

where the left-handed lepton doublets transform as 1, 1' and 1'' under A_4 , while the right-handed charged leptons are singlets. After electroweak symmetry breaking, the charged-lepton mass matrix is diagonal,

$$M_\ell = v \begin{pmatrix} y_\ell^{ee} & 0 & 0 \\ 0 & y_\ell^{\mu\mu} & 0 \\ 0 & 0 & y_\ell^{\tau\tau} \end{pmatrix} = \begin{pmatrix} m_e & 0 & 0 \\ 0 & m_\mu & 0 \\ 0 & 0 & m_\tau \end{pmatrix}, \quad (\text{A.2})$$

implying a trivial charged-lepton diagonalization matrix, $U_\ell = \mathbf{I}$.

Double Seesaw Lagrangian with A_4 Symmetry: The relevant leptonic mass terms of the double seesaw mechanism are described by the Lagrangian

$$\mathcal{L}_{\text{DSM}} = -\bar{L}_L \tilde{H} Y_D N_R - \bar{N}_R M_{RS} S_L - \frac{1}{2} \bar{S}_L^c M_S S_L + \text{h.c.}, \quad (\text{A.3})$$

where N_R denotes the right-handed neutrinos transforming as an A_4 triplet, S_L represents sterile fermions, and $\tilde{H} = i\sigma_2 H^*$.

Dirac Neutrino Mass Matrix M_D : Due to the A_4 charge assignments, the Dirac Yukawa coupling $\overline{L}_L \tilde{H} N_R$ is diagonal, yielding

$$M_D = v \begin{pmatrix} \alpha_D & 0 & 0 \\ 0 & \beta_D & 0 \\ 0 & 0 & \gamma_D \end{pmatrix}. \quad (\text{A.4})$$

In the degenerate Yukawa limit considered in the main text, one has $\alpha_D = \beta_D = \gamma_D \equiv \kappa_D$.

Right-Handed–Sterile Mixing Matrix M_{RS} : The mixing between N_R and S_L is described by

$$M_{RS} = v \begin{pmatrix} \alpha_{RS} & 0 & 0 \\ 0 & \beta_{RS} & 0 \\ 0 & 0 & \gamma_{RS} \end{pmatrix}, \quad (\text{A.5})$$

where v_T is the vacuum expectation value associated with the sterile sector. In the degenerate limit, $\alpha_{RS} = \beta_{RS} = \gamma_{RS} \equiv \kappa_{RS}$.

Sterile-Sector Majorana Mass Matrix M_S : The sterile-sector Majorana mass matrix is chosen to consist of an A_4 -symmetric leading term and a controlled symmetry-breaking correction,

$$M_S = M_S^{(0)} + M_S^{(\text{corr})}, \quad (\text{A.6})$$

with

$$M_S^{(0)} = \begin{pmatrix} b + \frac{2a}{3} & -\frac{a}{3} & -\frac{a}{3} \\ -\frac{a}{3} & \frac{2a}{3} & b - \frac{a}{3} \\ -\frac{a}{3} & b - \frac{a}{3} & \frac{2a}{3} \end{pmatrix}, \quad M_S^{(\text{corr})} = \begin{pmatrix} 0 & 0 & d \\ 0 & d & 0 \\ d & 0 & 0 \end{pmatrix}. \quad (\text{A.7})$$

The leading term $M_S^{(0)}$ is exactly diagonalized by the tribimaximal mixing matrix U_{TBM} , while the correction $M_S^{(\text{corr})}$ induces a nontrivial 1–3 rotation. This structure is responsible for generating a nonzero reactor mixing angle and leptonic CP violation.

Effective Light Neutrino Mass Matrix: After integrating out the heavy degrees of freedom, the effective light neutrino mass matrix is given by the double seesaw formula

$$m_\nu = M_D (M_{RS}^{-1})^T M_S M_{RS}^{-1} M_D^T. \quad (\text{A.8})$$

In the degenerate Yukawa limit, this expression reduces to

$$m_\nu = \kappa_\nu M_S, \quad \kappa_\nu = \left(\frac{v^2}{v_T^2} \right) \left(\frac{\kappa_D^2}{\kappa_{RS}^2} \right), \quad (\text{A.9})$$

which makes explicit that all flavor structure originates from M_S , while the overall neutrino mass scale is governed by the single parameter κ_ν . This decomposition provides the foundation for the analytic diagonalization and phenomenological analysis presented in the main text.

B Detailed Derivation of Mass and Mixing Structure in the Double Seesaw Framework with A_4 Symmetry

In this section, we present a detailed analytic derivation of the mass eigenvalues, mixing angles, and phases arising from the sterile-sector Majorana mass matrix M_S in the double seesaw framework endowed with an A_4 flavor symmetry. The construction is such that the flavor structure of M_S naturally separates into an A_4 -symmetric leading term and a controlled symmetry-breaking correction, allowing for a transparent diagonalization procedure.

Structure of the sterile-sector Majorana mass matrix

In the A_4 -symmetric realization of the model, the sterile-sector Majorana mass matrix can be written as

$$M_S = M_S^{(0)} + M_S^{(\text{corr})}, \quad (\text{B.1})$$

with

$$M_S^{(0)} = \begin{pmatrix} b + \frac{2a}{3} & -\frac{a}{3} & -\frac{a}{3} \\ -\frac{a}{3} & \frac{2a}{3} & b - \frac{a}{3} \\ -\frac{a}{3} & b - \frac{a}{3} & \frac{2a}{3} \end{pmatrix}, \quad M_S^{(\text{corr})} = \begin{pmatrix} 0 & 0 & d \\ 0 & d & 0 \\ d & 0 & 0 \end{pmatrix}. \quad (\text{B.2})$$

The leading term $M_S^{(0)}$ arises from A_4 triplet contractions of the type $\mathbf{3} \otimes \mathbf{3} \rightarrow \mathbf{1}$ and is exactly diagonalized by the tribimaximal mixing matrix U_{TBM} . The correction term $M_S^{(\text{corr})}$ softly breaks the A_4 symmetry and introduces off-diagonal entries that generate deviations from exact tribimaximal mixing.

Since in the degenerate Yukawa limit one has $M_D \propto M_{RS} \propto \mathbf{I}$, the same unitary transformation that diagonalizes M_S also diagonalizes the effective light neutrino mass matrix (up to an overall scaling factor). Therefore, the diagonalization of M_S fully determines the neutrino mixing structure.

Transformation to the TBM basis

Transforming M_S to the TBM basis, we obtain

$$\begin{aligned} M'_S &\equiv U_{\text{TBM}}^T M_S U_{\text{TBM}} \\ &= \begin{pmatrix} a + b - \frac{d}{2} & 0 & -\frac{\sqrt{3}}{2}d \\ 0 & b + d & 0 \\ -\frac{\sqrt{3}}{2}d & 0 & a - b + \frac{d}{2} \end{pmatrix}. \end{aligned} \quad (\text{B.3})$$

The transformed matrix exhibits a nontrivial structure only in the 1–3 block, while the (2, 2) entry remains diagonal. Consequently, the full diagonalization requires only a single rotation in the 1–3 plane.

Diagonalization via a single 1–3 rotation

The matrix M'_S can be diagonalized by a unitary rotation $U_{13}(\theta, \psi)$, such that

$$\begin{aligned} M_S^{\text{diag}} &= U_{13}^T M'_S U_{13} = (U_{13} U_{\text{TBM}})^T M_S (U_{\text{TBM}} U_{13}) \\ &= \text{diag}(M_{S_1} e^{i\phi_1}, M_{S_2} e^{i\phi_2}, M_{S_3} e^{i\phi_3}). \end{aligned} \quad (\text{B.4})$$

Requiring the off-diagonal (1, 3) element to vanish yields the condition

$$\tan 2\theta = \frac{2\sqrt{2}(a - b)}{a + b - 2d}, \quad (\text{B.5})$$

which determines the mixing angle associated with the 1–3 rotation.

Eigenvalues of the sterile-sector mass matrix

The resulting eigenvalues of M_S are given by

$$\begin{aligned} M_{S_1} &= a + \sqrt{b^2 + d^2 - bd}, \\ M_{S_2} &= b + d, \\ M_{S_3} &= a - \sqrt{b^2 + d^2 - bd}, \end{aligned} \quad (\text{B.6})$$

where the associated phases $\phi_{1,2,3}$ arise from the complex nature of the parameters a , b , and d .

To make the phase dependence explicit, we introduce the dimensionless ratios

$$\frac{d}{b} = \lambda_1 e^{i\phi_{db}}, \quad \frac{a}{b} = \lambda_2 e^{i\phi_{ab}}, \quad (\text{B.7})$$

with $\phi_{ab} = \phi_a - \phi_b$ and $\phi_{db} = \phi_d - \phi_b$. In terms of these parameters, the eigenvalues can be written as

$$\begin{aligned} M_{S_1} &= b \left[\lambda_2 e^{i\phi_{ab}} + \sqrt{1 + \lambda_1^2 e^{2i\phi_{db}} - \lambda_1 e^{i\phi_{db}}} \right], \\ M_{S_2} &= b(1 + \lambda_1 e^{i\phi_{db}}), \\ M_{S_3} &= b \left[\lambda_2 e^{i\phi_{ab}} - \sqrt{1 + \lambda_1^2 e^{2i\phi_{db}} - \lambda_1 e^{i\phi_{db}}} \right]. \end{aligned} \quad (\text{B.8})$$

This analytic structure demonstrates explicitly how the sterile-sector masses, mixing angles, and CP-violating phases are governed by the A_4 symmetry and its controlled breaking. The presence of a single complex rotation explains the origin of nonzero reactor mixing and leptonic CP violation in a minimal and predictive manner, providing the foundation for the phenomenological analysis presented in the main text.

C Flavon Potential and Vacuum Alignment

In this section, we discuss the scalar potential responsible for the spontaneous breaking of the A_4 flavor symmetry and the resulting vacuum alignments that lead to predictive mass textures in the double seesaw framework. The flavon fields ϕ_T , ϕ_S , ξ , and ξ' play distinct and complementary roles in shaping the charged-lepton and neutrino mass structures. In particular, the alignment of ϕ_T enforces a diagonal structure for the Dirac mass matrix M_D and the right-handed-sterile mixing matrix M_{RS} , while the combined alignments of ϕ_S , ξ , and ξ' determine the flavor structure of the sterile-sector Majorana mass matrix M_S . Since, in the degenerate Yukawa limit, the effective light neutrino mass matrix satisfies $m_\nu = \kappa_\nu M_S$, the entire flavor structure of light neutrinos is governed by the vacuum alignment in the sterile sector [57–60].

The most general renormalizable scalar potential invariant under $A_4 \times SU(2)_L \times U(1)_Y$ can be written as

$$V = V_T + V_S + V_\xi + V_{\xi'} + V_{\text{mix}}, \quad (\text{C.1})$$

where each term corresponds to self-interactions or mutual interactions among the flavon fields, as discussed below.

Triplet Potential for ϕ_T

The A_4 -invariant scalar potential for the flavon triplet ϕ_T is given by

$$V_T = \mu_T^2 (\phi_T \cdot \phi_T) + \lambda_1 (\phi_T \cdot \phi_T)^2 + \lambda_2 (\phi_T \cdot \phi_T)_{1'} (\phi_T \cdot \phi_T)_{1''} + \lambda_3 (\phi_T \cdot \phi_T)_{3_s} \cdot (\phi_T \cdot \phi_T)_{3_s}, \quad (\text{C.2})$$

where (\dots) denotes contractions into the corresponding A_4 representations. Minimization of V_T yields

$$\frac{\partial V_T}{\partial \phi_{T1}} = 0 \quad \Rightarrow \quad v_T^2 = -\frac{\mu_T^2}{2\lambda_1}, \quad (\text{C.3})$$

with $\partial V_T / \partial \phi_{T2,3} = 0$. The resulting vacuum alignment is

$$\langle \phi_T \rangle = (v_T, 0, 0), \quad (\text{C.4})$$

which preserves the Z_3 subgroup of A_4 . This alignment ensures that both the Dirac neutrino mass matrix M_D and the right-handed-sterile mixing matrix M_{RS} are diagonal, thereby eliminating any source of flavor mixing from these sectors.

Triplet Potential for ϕ_S

The triplet flavon ϕ_S governs the neutrino mass sector. Its most general A_4 -invariant potential is

$$V_S = \mu_S^2 (\phi_S \cdot \phi_S) + \kappa_1 (\phi_S \cdot \phi_S)^2 + \kappa_2 (\phi_S \cdot \phi_S)_{1'} (\phi_S \cdot \phi_S)_{1''} + \kappa_3 (\phi_S \cdot \phi_S)_{3_s} \cdot (\phi_S \cdot \phi_S)_{3_s}. \quad (\text{C.5})$$

Minimization yields

$$v_S^2 = -\frac{\mu_S^2}{2(\kappa_1 + \kappa_3)}, \quad (\text{C.6})$$

leading to the democratic alignment

$$\langle \phi_S \rangle = (v_S, v_S, v_S). \quad (\text{C.7})$$

This alignment preserves a residual Z_2 symmetry and generates the tribimaximal structure of the sterile-sector mass matrix $M_S^{(0)}$, which in turn determines the leading-order structure of the light neutrino mass matrix.

Singlet Flavons ξ and ξ'

The singlet flavons ξ and ξ' provide additional contributions to the neutrino sector through their couplings to ϕ_S . Their self-interaction potentials are

$$V_\xi = \mu_\xi^2 \xi^2 + \lambda_\xi \xi^4, \quad V_{\xi'} = \mu_{\xi'}^2 \xi'^2 + \lambda_{\xi'} \xi'^4. \quad (\text{C.8})$$

Minimization yields the vacuum expectation values

$$\langle \xi \rangle = u, \quad \langle \xi' \rangle = u'. \quad (\text{C.9})$$

While ξ contributes to the leading TBM structure of M_S , the singlet ξ' induces controlled symmetry-breaking corrections, generating deviations from exact tribimaximal mixing and enabling a nonzero reactor angle θ_{13} .

Mixed Interaction Terms

The mixed flavon interactions are described by

$$V_{\text{mix}} = \alpha(\phi_T \cdot \phi_T)(\phi_S \cdot \phi_S) + \beta(\phi_T \cdot \phi_T)\xi^2 + \gamma_3(\phi_S \cdot \phi_S)\xi^2 + \gamma_4(\phi_S \cdot \phi_S)\xi'^2 + \gamma_5\xi^2\xi'^2, \quad (\text{C.10})$$

which stabilize the vacuum configuration and correlate the magnitudes of the VEVs without altering the alignment directions.

Summary of Vacuum Alignments

The minimization of the full scalar potential leads to the vacuum structure

$$\langle \phi_T \rangle = (v_T, 0, 0), \quad \langle \phi_S \rangle = (v_S, v_S, v_S), \quad \langle \xi \rangle = u, \quad \langle \xi' \rangle = u'. \quad (\text{C.11})$$

These alignments and their roles in the double seesaw framework are summarized in Table 4.

Table 4: Flavon vacuum alignments and their roles in the double seesaw framework.

Flavon	VEV Alignment	Role
ϕ_T	$(v_T, 0, 0)$	Enforces diagonal M_D and M_{RS}
ϕ_S, ξ	$(v_S, v_S, v_S), u$	Generates TBM structure of M_S and m_ν
ξ'	u'	Provides controlled corrections to M_S and m_ν

In summary, the vacuum alignment enforced by the A_4 symmetry ensures that all lepton flavor mixing originates exclusively from the sterile-sector Majorana mass matrix M_S . This feature renders the double seesaw framework highly predictive: the charged-lepton, Dirac, and right-handed-sterile sectors remain flavor diagonal, while the observed neutrino mixing and CP violation emerge solely from the structure and controlled breaking of M_S .

D Detailed Derivation of Mixing Angles and CP Phases

In this appendix, we present the detailed analytic derivation of the neutrino mixing angles and CP-violating phases arising in the double seesaw-invoked A_4 framework. The purpose of this section is to provide a transparent derivation of the relations quoted in the main text.

Diagonalization of the 1–3 Subspace

After transforming the sterile-sector mass matrix into the tribimaximal basis, the effective matrix in the 1–3 subspace takes the form

$$M = \begin{pmatrix} X & Y \\ Y & Z \end{pmatrix}, \quad (\text{D.1})$$

where

$$X = a + b - \frac{d}{2}, \quad Y = \frac{\sqrt{3}}{2} d, \quad Z = a - b + \frac{d}{2}. \quad (\text{D.2})$$

This matrix can be diagonalized by a unitary rotation in the 1–3 plane,

$$R = \begin{pmatrix} \cos \theta & \sin \theta e^{-i\psi} \\ -\sin \theta e^{i\psi} & \cos \theta \end{pmatrix}, \quad (\text{D.3})$$

where θ is the rotation angle and ψ is a CP-violating phase.

The condition that the off-diagonal element of $R^T M R$ vanishes leads to

$$Y \cos 2\theta + \sin \theta \cos \theta \left[\cos \psi (X - Z) - i \sin \psi (X + Z) \right] = 0. \quad (\text{D.4})$$

This yields

$$\frac{\tan 2\theta}{2} = \frac{Y}{\cos \psi (Z - X) + i \sin \psi (X + Z)}. \quad (\text{D.5})$$

Dimensionless Parametrization

To simplify the analysis, we normalize all quantities with respect to b and define

$$\frac{a}{b} = \lambda_2 e^{i\phi_{ab}}, \quad \frac{d}{b} = \lambda_1 e^{i\phi_{db}}, \quad (\text{D.6})$$

with b chosen real and positive. The dimensionless parameters then become

$$\tilde{X} = \lambda_2 e^{i\phi_{ab}} + 1 - \frac{\lambda_1}{2} e^{i\phi_{db}}, \quad (\text{D.7})$$

$$\tilde{Y} = \frac{\sqrt{3}}{2} \lambda_1 e^{i\phi_{db}}, \quad (\text{D.8})$$

$$\tilde{Z} = \lambda_2 e^{i\phi_{ab}} - 1 + \frac{\lambda_1}{2} e^{i\phi_{db}}. \quad (\text{D.9})$$

From these expressions,

$$\tilde{X} + \tilde{Z} = 2\lambda_2 e^{i\phi_{ab}}, \quad \tilde{Z} - \tilde{X} = \lambda_1 e^{i\phi_{db}} - 2. \quad (\text{D.10})$$

Substituting into Eq. (D.5) yields

$$\tan 2\theta = \frac{\sqrt{3}\lambda_1 e^{i\phi_{db}}}{2i\lambda_2 e^{i\phi_{ab}} \sin \psi + (\lambda_1 e^{i\phi_{db}} - 2) \cos \psi}. \quad (\text{D.11})$$

Separating the real part gives

$$\boxed{\tan 2\theta = \frac{\sqrt{3}\lambda_1 \cos \phi_{db}}{\lambda_1 \cos \psi \cos \phi_{db} - 2(\lambda_2 \sin \psi \sin \phi_{ab} + \cos \psi)}}. \quad (\text{D.12})$$

Determination of the CP Phase ψ

Requiring the imaginary part of the denominator to vanish leads to

$$\lambda_2 \sin \psi \cos(\phi_{ab} - \phi_{db}) + \cos \psi \sin \phi_{db} = 0, \quad (\text{D.13})$$

which yields

$$\boxed{\tan \psi = -\frac{\sin \phi_{db}}{\lambda_2 \cos(\phi_{ab} - \phi_{db})}}. \quad (\text{D.14})$$

Connection to PMNS Parameters

Since the charged-lepton mass matrix is diagonal, $U_\ell = \mathbf{I}$, the PMNS matrix coincides with the neutrino diagonalization matrix,

$$U_{\text{PMNS}} = U_{\text{TBM}} U_{13}(\theta, \psi) U_m. \quad (\text{D.15})$$

Comparing with the standard PDG parametrization yields

$$\boxed{\sin \theta_{13} = \sqrt{\frac{2}{3}} |\sin \theta|}. \quad (\text{D.16})$$

For $\sin \theta > 0$, one obtains

$$\boxed{\delta_{\text{CP}} = \psi}, \quad (\text{D.17})$$

while for $\sin \theta < 0$, $\delta_{\text{CP}} = \psi + \pi$. In both cases, $\tan \delta_{\text{CP}} = \tan \psi$, and hence

$$\boxed{\tan \delta_{\text{CP}} = -\frac{\sin \phi_{db}}{\lambda_2 \cos(\phi_{ab} - \phi_{db})}}. \quad (\text{D.18})$$

The remaining mixing angles follow as

$$\boxed{\theta_{12} = \sin^{-1} \left(\frac{1}{\sqrt{3} \cos \theta_{13}} \right)}, \quad (\text{D.19})$$

and

$$\boxed{\tan \theta_{23} = \frac{-\frac{\cos \theta}{\sqrt{2}} - \frac{e^{-i\psi} \sin \theta}{\sqrt{6}}}{\frac{\cos \theta}{\sqrt{2}} - \frac{e^{-i\psi} \sin \theta}{\sqrt{6}}}}. \quad (\text{D.20})$$

These expressions demonstrate explicitly that all lepton mixing angles and the Dirac CP phase are controlled by a single rotation angle θ and a single phase ψ , which originate from the A_4 -breaking structure of the sterile sector in the double seesaw mechanism.

References

- [1] **SNO**, Q. R. Ahmad et al., *Direct evidence for neutrino flavor transformation from neutral current interactions in the Sudbury Neutrino Observatory*, *Phys. Rev. Lett.* **89** (2002) 011301, [[nucl-ex/0204008](#)].
- [2] **T2K**, K. Abe et al., *Search for light sterile neutrinos with the T2K far detector Super-Kamiokande at a baseline of 295 km*, *Phys. Rev. D* **99** (2019), no. 7 071103, [[1902.06529](#)].
- [3] **Daya Bay**, F. P. An et al., *Observation of electron-antineutrino disappearance at Daya Bay*, *Phys. Rev. Lett.* **108** (2012) 171803, [[1203.1669](#)].
- [4] **Double Chooz**, Y. Abe et al., *Indication of Reactor $\bar{\nu}_e$ Disappearance in the Double Chooz Experiment*, *Phys. Rev. Lett.* **108** (2012) 131801, [[1112.6353](#)].
- [5] P. Minkowski, $\mu \rightarrow e\gamma$ at a Rate of One Out of 10^9 Muon Decays?, *Phys. Lett. B* **67** (1977) 421–428.
- [6] R. N. Mohapatra and G. Senjanovic, *Neutrino Mass and Spontaneous Parity Nonconservation*, *Phys. Rev. Lett.* **44** (1980) 912.
- [7] T. Yanagida, *Horizontal gauge symmetry and masses of neutrinos*, *Conf. Proc. C* **7902131** (1979) 95–99.
- [8] M. Gell-Mann, P. Ramond, and R. Slansky, *Complex Spinors and Unified Theories*, *Conf. Proc. C* **790927** (1979) 315–321, [[1306.4669](#)].
- [9] M. Fukugita and T. Yanagida, *Baryogenesis Without Grand Unification*, *Phys. Lett. B* **174** (1986) 45–47.

[10] M. Magg and C. Wetterich, *Neutrino Mass Problem and Gauge Hierarchy*, *Phys. Lett.* **B94** (1980) 61–64.

[11] J. Schechter and J. W. F. Valle, *Neutrino Masses in $SU(2) \times U(1)$ Theories*, *Phys. Rev. D* **22** (1980) 2227.

[12] T. P. Cheng and L.-F. Li, *Neutrino Masses, Mixings and Oscillations in $SU(2) \times U(1)$ Models of Electroweak Interactions*, *Phys. Rev. D* **22** (1980) 2860.

[13] G. Lazarides, Q. Shafi, and C. Wetterich, *Proton Lifetime and Fermion Masses in an $SO(10)$ Model*, *Nucl. Phys.* **B181** (1981) 287–300.

[14] R. N. Mohapatra and G. Senjanovic, *Neutrino Masses and Mixings in Gauge Models with Spontaneous Parity Violation*, *Phys. Rev. D* **23** (1981) 165.

[15] R. Foot, H. Lew, X. G. He, and G. C. Joshi, *Seesaw Neutrino Masses Induced by a Triplet of Leptons*, *Z. Phys. C* **44** (1989) 441.

[16] B. He, N. Okada, and Q. Shafi, *125 GeV Higgs, type III seesaw and gauge–Higgs unification*, *Phys. Lett. B* **716** (2012) 197–202, [[1205.4038](#)].

[17] **SNO**, Q. R. Ahmad et al., *Measurement of the rate of $\nu_e + d \rightarrow p + p + e^-$ interactions produced by 8B solar neutrinos at the Sudbury Neutrino Observatory*, *Phys. Rev. Lett.* **87** (2001) 071301, [[nucl-ex/0106015](#)].

[18] **KamLAND**, K. Eguchi et al., *First results from KamLAND: Evidence for reactor anti-neutrino disappearance*, *Phys. Rev. Lett.* **90** (2003) 021802, [[hep-ex/0212021](#)].

[19] **Super-Kamiokande**, Y. Fukuda et al., *Evidence for oscillation of atmospheric neutrinos*, *Phys. Rev. Lett.* **81** (1998) 1562–1567, [[hep-ex/9807003](#)].

[20] P. A. M. Dirac, *The quantum theory of the electron*, *Proc. Roy. Soc. Lond. A* **117** (1928) 610–624.

[21] E. Majorana, *Teoria simmetrica dell'elettrone e del positrone*, *Nuovo Cim.* **14** (1937) 171–184.

[22] M. Hirsch, S. Morisi, and J. W. F. Valle, *A4-based tri-bimaximal mixing within inverse and linear seesaw schemes*, *Phys. Lett. B* **679** (2009) 454–459, [[0905.3056](#)].

[23] P.-H. Gu and U. Sarkar, *Leptogenesis with Linear, Inverse or Double Seesaw*, *Phys. Lett. B* **694** (2011) 226–232, [[1007.2323](#)].

[24] P. S. B. Dev and R. N. Mohapatra, *TeV Scale Inverse Seesaw in $SO(10)$ and Leptonic Non-Unitarity Effects*, *Phys. Rev. D* **81** (2010) 013001, [[0910.3924](#)].

[25] F. F. Deppisch, L. Graf, S. Kulkarni, S. Patra, W. Rodejohann, et al., *Reconciling the 2 TeV excesses at the LHC in a linear seesaw left-right model*, *Phys. Rev. D* **93** (2016), no. 1 013011, [[1508.05940](#)].

[26] P. Humbert, M. Lindner, S. Patra, and J. Smirnov, *Lepton Number Violation within the Conformal Inverse Seesaw*, *JHEP* **09** (2015) 064, [[1505.07453](#)].

[27] M. K. Parida and S. Patra, *Left-right models with light neutrino mass prediction and dominant neutrinoless double beta decay rate*, *Phys. Lett. B* **718** (2013) 1407–1412, [[1211.5000](#)].

[28] V. Brdar and A. Y. Smirnov, *Low Scale Left-Right Symmetry and Naturally Small Neutrino Mass*, *JHEP* **02** (2019) 045, [[1809.09115](#)].

[29] M. Thomas Arun, T. Mandal, S. Mitra, A. Mukherjee, L. Priya, et al., *Testing left-right symmetry with an inverse seesaw mechanism at the LHC*, *Phys. Rev. D* **105** (2022), no. 11 115007, [[2109.09585](#)].

[30] P. Sahu, S. Patra, and P. Pritimita, *Neutrino mass and lepton flavor violation in A_4 -based left-right symmetric model with linear seesaw*, *Int. J. Mod. Phys. A* **37** (2022), no. 06 2250030.

[31] K. Ezzat, M. Ashry, and S. Khalil, *Search for a heavy neutral Higgs boson in a left-right model with an inverse seesaw mechanism at the LHC*, *Phys. Rev. D* **104** (2021), no. 1 015016, [[2101.08255](#)].

[32] R. N. Mohapatra et al., *Theory of Neutrinos: A White Paper*, *Rept. Prog. Phys.* **70** (2007) 1757–1867, [[hep-ph/0510213](#)].

[33] R. N. Mohapatra, *Mechanism for Understanding Small Neutrino Mass in Superstring Theories*, *Phys. Rev. Lett.* **56** (1986) 561–563.

[34] R. N. Mohapatra and J. W. F. Valle, *Neutrino Mass and Baryon Number Nonconservation in Superstring Models*, *Phys. Rev. D* **34** (1986) 1642.

[35] M. Malinsky, J. C. Romao, and J. W. F. Valle, *Novel supersymmetric $SO(10)$ seesaw mechanism*, *Phys. Rev. Lett.* **95** (2005) 161801, [[hep-ph/0506296](#)].

[36] J. Kersten and A. Y. Smirnov, *Right-Handed Neutrinos at CERN LHC and the Mechanism of Neutrino Mass Generation*, *Phys. Rev. D* **76** (2007) 073005, [[0705.3221](#)].

[37] S. Patra, S. T. Petcov, P. Pritimita, and P. Sahu, *Neutrinoless double beta decay in a left-right symmetric model with a double seesaw mechanism*, *Phys. Rev. D* **107** (2023), no. 7 075037, [[2302.14538](#)].

[38] P. Adarsh, R. Banerjee, P. Sahu, U. Patel, and S. Patra, *Probing $0\nu\beta\beta$ and $\mu \rightarrow e\gamma$ via Fully Determined Dirac Mass Terms in LRSM with Double Seesaw*, [2508.15893](#).

[39] U. Patel, P. Adarsh, S. Patra, and P. Sahu, *Leptogenesis in a Left-Right Symmetric Model with double seesaw*, *JHEP* **03** (2024) 029, [[2310.09337](#)].

[40] **JUNO**, A. Abusleme et al., *First measurement of reactor neutrino oscillations at JUNO*, [2511.14593](#).

[41] D. Zhang, *Trimaximal Mixing Patterns Meet the First JUNO Result*, [2511.15654](#).

[42] K. S. Babu, E. Ma, and J. W. F. Valle, *Underlying $A(4)$ symmetry for the neutrino mass matrix and the quark mixing matrix*, *Phys. Lett. B* **552** (2003) 207–213, [[hep-ph/0206292](#)].

[43] E. Ma, *$A(4)$ symmetry and neutrinos with very different masses*, *Phys. Rev. D* **70** (2004) 031901, [[hep-ph/0404199](#)].

[44] S. K. Kang, Z.-z. Xing, and S. Zhou, *Possible deviation from the tri-bimaximal neutrino mixing in a seesaw model*, *Phys. Rev. D* **73** (2006) 013001, [[hep-ph/0511157](#)].

[45] S. K. Nanda, M. Ricky Devi, and S. Patra, *Non-Holomorphic A_4 Modular Symmetry in Type-I Seesaw: Implications for Neutrino Masses and Leptogenesis*, [2509.22108](#).

[46] M. R. Devi, *Retrieving texture zeros in 3+1 active-sterile neutrino framework under the action of A_4 modular-invariants*, [2303.04900](#).

[47] M. Ricky Devi, *Neutrino Masses and Higher Degree Siegel Modular Forms*, [2401.16257](#).

[48] S. Centelles Chuliá and R. Kumar, *Minimal A_4 Type-II Seesaw Realization of Testable Neutrino Mass Sum Rules*, [2512.22343](#).

[49] R. Kumar, N. Nath, R. Srivastava, and S. Yadav, *Dirac Scoto inverse-seesaw from A_4 flavor symmetry*, *JHEP* **10** (2025) 088, [[2505.01407](#)].

[50] R. Kumar, N. Nath, and R. Srivastava, *Cutting the Scotogenic Loop: A_4 Flavor Symmetry to Z_2 Dark Symmetry*, *Springer Proc. Phys.* **304** (2024) 1183–1185.

[51] M. R. Devi and K. Bora, *Octant of θ_{23} , MH , $0\nu\beta\beta$ decay and vacuum alignment of A_4 flavor symmetry in an inverse seesaw model*, *Mod. Phys. Lett. A* **37** (2022), no. 12 2250073, [[2112.13004](#)].

[52] M. R. Devi and K. Bora, *Exploring the feasibility of the charged lepton flavor violating decay $\mu \rightarrow e + \gamma$ in inverse and linear seesaw mechanisms with A_4 flavor symmetry*, *Mod. Phys. Lett. A* **37** (2022), no. 31 2250206, [[2208.02214](#)].

[53] M. Kashav and S. Verma, *A_4 Flavor Model for Deviation in $\mu - \tau$ Reflection Symmetry with Type-I+II Seesaw Extensions*, *Int. J. Theor. Phys.* **62** (2023), no. 12 267.

[54] R. Verma, M. Kashav, S. Verma, and B. C. Chauhan, *Scalar dark matter in the A_4 -based texture one-zero neutrino mass model within the inverse seesaw mechanism*, *PTEP* **2021** (2021), no. 12 123B01, [[2102.03074](#)]. [Erratum: PTEP 2022, 039301 (2022)].

[55] S. Verma, M. Kashav, and S. Bhardwaj, *Highly predictive and testable A_4 flavor model within type-I and II seesaw framework and associated phenomenology*, *Nucl. Phys. B* **946** (2019) 114704, [[1811.06249](#)].

[56] W. Grimus and L. Lavoura, *The Seesaw mechanism at arbitrary order: Disentangling the small scale from the large scale*, *JHEP* **11** (2000) 042, [[hep-ph/0008179](#)].

[57] G. Altarelli and F. Feruglio, *Tri-bimaximal neutrino mixing from discrete symmetry in extra dimensions*, *Nucl. Phys. B* **720** (2005) 64–88, [[hep-ph/0504165](#)].

[58] G. Altarelli and F. Feruglio, *Tri-bimaximal neutrino mixing, $A(4)$ and the modular symmetry*, *Nucl. Phys. B* **741** (2006) 215–235, [[hep-ph/0512103](#)].

[59] E. Ma and G. Rajasekaran, *Softly broken $A(4)$ symmetry for nearly degenerate neutrino masses*, *Phys. Rev. D* **64** (2001) 113012, [[hep-ph/0106291](#)].

[60] W. Grimus and L. Lavoura, *Double seesaw mechanism and lepton mixing*, *JHEP* **03** (2014) 004, [[1309.3186](#)].

[61] A. Y. Smirnov, *Seesaw enhancement of lepton mixing*, *Phys. Rev. D* **48** (1993) 3264–3270, [[hep-ph/9304205](#)].

[62] G. Altarelli and F. Feruglio, *Models of neutrino masses and mixings*, *New J. Phys.* **6** (2004) 106, [[hep-ph/0405048](#)].

[63] M. Lindner, M. A. Schmidt, and A. Y. Smirnov, *Screening of Dirac flavor structure in the seesaw and neutrino mixing*, *JHEP* **07** (2005) 048, [[hep-ph/0505067](#)].

[64] P. O. Ludl and A. Y. Smirnov, *Lepton mixing from the hidden sector*, *Phys. Rev. D* **92** (2015), no. 7 073010, [[1507.03494](#)].

[65] B. Bajc and A. Y. Smirnov, *Hidden flavor symmetries of $SO(10)$ GUT*, *Nucl. Phys. B* **909** (2016) 954–979, [[1605.07955](#)].

[66] A. Y. Smirnov and X.-J. Xu, *Neutrino mixing in $SO(10)$ GUTs with a non-Abelian flavor symmetry in the hidden sector*, *Phys. Rev. D* **97** (2018), no. 9 095030, [[1803.07933](#)].

[67] U. Patel, P. Adarsh, S. Patra, and P. Sahu, *Leptogenesis in a Left-Right Symmetric Model with double seesaw*, *EPJ Web Conf.* **312** (2024) 02008.

[68] S. Davidson, E. Nardi, and Y. Nir, *Leptogenesis*, *Phys. Rept.* **466** (2008) 105–177, [[0802.2962](#)].

[69] M. A. Luty, *Baryogenesis via leptogenesis*, *Phys. Rev. D* **45** (1992) 455–465.

[70] L. Covi, E. Roulet, and F. Vissani, *CP violating decays in leptogenesis scenarios*, *Phys. Lett. B* **384** (1996) 169–174, [[hep-ph/9605319](#)].

[71] P. S. B. Dev, P. Di Bari, B. Garbrecht, S. Lavignac, P. Millington, et al., *Flavor effects in leptogenesis*, *Int. J. Mod. Phys. A* **33** (2018) 1842001, [[1711.02861](#)].

[72] I. Esteban, M. C. Gonzalez-Garcia, M. Maltoni, I. Martinez-Soler, J. P. Pinheiro, et al., *NuFit-6.0: updated global analysis of three-flavor neutrino oscillations*, *JHEP* **12** (2024) 216, [[2410.05380](#)].

[73] **KamLAND**, A. Gando et al., *Reactor On-Off Antineutrino Measurement with KamLAND*, *Phys. Rev. D* **88** (2013), no. 3 033001, [[1303.4667](#)].

[74] **Super-Kamiokande**, K. Abe et al., *Solar neutrino measurements using the full data period of Super-Kamiokande-IV*, *Phys. Rev. D* **109** (2024), no. 9 092001, [[2312.12907](#)].

[75] **SNO+**, M. Abreu et al., *Measurement of reactor antineutrino oscillations with 1.46 ktonne-years of data at SNO+*, [2511.11856](#).

[76] **(IceCube Collaboration) II**, IceCube, R. Abbasi et al., *Measurement of Atmospheric Neutrino Oscillation Parameters Using Convolutional Neural Networks with 9.3 Years of Data in IceCube DeepCore*, *Phys. Rev. Lett.* **134** (2025), no. 9 091801, [[2405.02163](#)].

[77] **Super-Kamiokande**, T. Wester et al., *Atmospheric neutrino oscillation analysis with neutron tagging and an expanded fiducial volume in Super-Kamiokande I–V*, *Phys. Rev. D* **109** (2024), no. 7 072014, [[2311.05105](#)].

[78] **NOvA**, S. Abubakar et al., *Precision measurement of neutrino oscillation parameters with 10 years of data from the NOvA experiment*, [[2509.04361](#)].

[79] **T2K, NOvA**, S. Abubakar et al., *Joint neutrino oscillation analysis from the T2K and NOvA experiments*, *Nature* **646** (2025), no. 8086 818–824, [[2510.19888](#)].

[80] **KM3NeT**, S. Aiello et al., *Measurement of neutrino oscillation parameters with the first six detection units of KM3NeT/ORCA*, *JHEP* **10** (2024) 206, [[2408.07015](#)]. [Addendum: *JHEP* 10, 041 (2025)].

[81] I. Esteban, M. C. Gonzalez-Garcia, M. Maltoni, I. Martinez-Soler, J. P. Pinheiro, et al., *Nufit-6.0: updated global analysis of three-flavor neutrino oscillations*, *JHEP* **12** (2024) 216, [[2410.05380](#)].

[82] **SNO**, B. Aharmim et al., *Combined Analysis of all Three Phases of Solar Neutrino Data from the Sudbury Neutrino Observatory*, *Phys. Rev. C* **88** (2013) 025501, [[1109.0763](#)].

[83] **Super-Kamiokande**, K. Abe et al., *Solar Neutrino Measurements in Super-Kamiokande-IV*, *Phys. Rev. D* **94** (2016), no. 5 052010, [[1606.07538](#)].

[84] GitLab/JINR, *Gitlab community edition of joint institute for nuclear research*, 2025.

[85] **T2K**, K. Abe et al., *Measurements of neutrino oscillation parameters from the T2K experiment using 3.6×10^{21} protons on target*, *Eur. Phys. J. C* **83** (2023), no. 9 782, [[2303.03222](#)].

[86] Neutrino-2024, *Xxxi international conference on neutrino physics and astrophysics (neutrino 2024)*, 2024.

[87] NNN23, *22nd international workshop on next generation nucleon decay and neutrino detectors (nnn23)*, 2023.

[88] **MINOS+**, P. Adamson et al., *Precision Constraints for Three-Flavor Neutrino Oscillations from the Full MINOS+ and MINOS Dataset*, *Phys. Rev. Lett.* **125** (2020), no. 13 131802, [[2006.15208](#)].

[89] A. G. et al. (KamLAND-Zen Collaboration), *Search for the majorana nature of neutrinos in the inverted mass ordering region with kamland-zen*, *Phys. Rev. Lett.* **130** (2023) 051801. $|m_{\beta\beta}| < 36\text{--}156$ meV at 90% C.L.

[90] **KamLAND-Zen**, S. Abe et al., *Search for Majorana Neutrinos with the Complete KamLAND-Zen Dataset*, [[2406.11438](#)].

[91] **GERDA**, M. Agostini et al., *Final Results of GERDA on the Search for Neutrinoless Double- β Decay*, *Phys. Rev. Lett.* **125** (2020), no. 25 252502, [[2009.06079](#)].

[92] **Planck**, N. Aghanim et al., *Planck 2018 results. VI. Cosmological parameters*, *Astron. Astrophys.* **641** (2020) A6, [[1807.06209](#)]. [Erratum: *Astron. Astrophys.* 652, C4 (2021)].

[93] **KATRIN**, M. Aker et al., *Direct neutrino-mass measurement based on 259 days of KATRIN data*, *Science* **388** (2025), no. 6743 adq9592, [[2406.13516](#)].

[94] S.-F. Ge, C.-F. Kong, M. Lindner, and J. P. Pinheiro, *Neutrinoless Double Beta Decay in Light of JUNO First Data*, [2511.15391](#).

[95] **LEGEND**, H. Acharya et al., *First Results on the Search for Lepton Number Violating Neutrinoless Double Beta Decay with the LEGEND-200 Experiment*, [2505.10440](#).

[96] **EXO-200**, G. Anton et al., *Search for Neutrinoless Double- β Decay with the Complete EXO-200 Dataset*, *Phys. Rev. Lett.* **123** (2019), no. 16 161802, [[1906.02723](#)].

[97] **CUORE**, D. Q. Adams et al., *Improved Limit on Neutrinoless Double-Beta Decay in ^{130}Te with CUORE*, *Phys. Rev. Lett.* **124** (2020), no. 12 122501, [[1912.10966](#)].

[98] **nEXO**, G. Adhikari et al., *nEXO: neutrinoless double beta decay search beyond 10^{28} year half-life sensitivity*, *J. Phys. G* **49** (2022), no. 1 015104, [[2106.16243](#)].

[99] **nEXO**, J. B. Albert et al., *Sensitivity and Discovery Potential of nEXO to Neutrinoless Double Beta Decay*, *Phys. Rev. C* **97** (2018), no. 6 065503, [[1710.05075](#)].

[100] **LEGEND**, N. Abgrall et al., *The Large Enriched Germanium Experiment for Neutrinoless $\beta\beta$ Decay: LEGEND-1000 Preconceptual Design Report*, [2107.11462](#).

[101] **CUPID**, A. Armatol et al., *Toward CUPID-1T*, [2203.08386](#).

[102] **CUPID**, E. Armengaud et al., *New Limit for Neutrinoless Double-Beta Decay of ^{100}Mo from the CUPID-Mo Experiment*, *Phys. Rev. Lett.* **126** (2021), no. 18 181802, [[2011.13243](#)].

[103] C. Jarlskog, *Commutator of the Quark Mass Matrices in the Standard Electroweak Model and a Measure of Maximal CP Nonconservation*, *Phys. Rev. Lett.* **55** (1985) 1039.

[104] I. Esteban, M. C. Gonzalez-Garcia, M. Maltoni, T. Schwetz, and A. Zhou, *The fate of hints: updated global analysis of three-flavor neutrino oscillations*, *JHEP* **09** (2020) 178, [[2007.14792](#)].

[105] S. F. King and C. Luhn, *Neutrino Mass and Mixing with Discrete Symmetry*, *Rept. Prog. Phys.* **76** (2013) 056201, [[1301.1340](#)].

[106] P. F. Harrison and W. G. Scott, *Symmetries and generalizations of tri - bimaximal neutrino mixing*, *Phys. Lett. B* **535** (2002) 163–169, [[hep-ph/0203209](#)].

[107] **JUNO**, F. An et al., *Neutrino Physics with JUNO*, *J. Phys. G* **43** (2016), no. 3 030401, [[1507.05613](#)].

[108] **JUNO**, A. Abusleme et al., *Sub-percent precision measurement of neutrino oscillation parameters with JUNO*, *Chin. Phys. C* **46** (2022), no. 12 123001, [[2204.13249](#)].